1   **Title:** Maturing Mycobacterial Peptidoglycan Requires Non-canonical Crosslinks

2   to Maintain Shape

3   **Authors:** Catherine Baranowski[1], Michael A. Welsh[2], Lok-To Sham[2,3], Haig A.

4   Eskandarian[4,5], Hoong C. Lim[2], Karen J. Kieser[1], Jeffrey C. Wagner[1], John D.

5   McKinney[4], Georg E. Fantner[5], Thomas R. Ioerger[6], Suzanne Walker[2], Thomas G.

6   Bernhardt[2], Eric J. Rubin[1,2]*, E. Hesper Rego[7*]

7   **Affiliations:**

8   [1] Department of Immunology and Infectious Disease, Harvard T. H. Chan School of Public

9   Health, Boston, MA 02115, USA; [2] Department of Microbiology and Immunobiology,

10 Harvard Medical School, Boston, MA 02115, USA; [3] Department of Microbiology and

11 Immunology, National University of Singapore, 117545 Singapore; [4] School of Life

12 Sciences, Swiss Federal Institute of Technology in Lausanne (EPFL), 1015 Lausanne,

13 Switzerland; [5] School of Engineering, Swiss Federal Institute of Technology in Lausanne

14 (EPFL), 1015 Lausanne, Switzerland; [6] Department of Computer Science and

15 Engineering, Texas A&M University, College Station, Texas, USA;[7] Department of

16 Microbial Pathogenesis, Yale University School of Medicine, New Haven, Connecticut,

17 06510, USA.

18 * to whom correspondence should be addressed: erubin@hsph.harvard.edu;

19 hesper.rego@yale.edu

20

21

22

23

Abstract:

In most well studied rod-shaped bacteria, peptidoglycan is primarily crosslinked by penicillin binding proteins (PBPs). However, in mycobacteria, L,D-transpeptidase (LDT)- mediated crosslinks are highly abundant. To elucidate the role of these unusual crosslinks, we characterized mycobacterial cells lacking all LDTs. We find that LDT- mediated crosslinks are required for rod shape maintenance specifically at sites of aging cell wall, a byproduct of polar elongation. Asymmetric polar growth leads to a non-uniform distribution of these two types of crosslinks in a single cell. Consequently, in the absence of LDT-mediated crosslinks, PBP-catalyzed crosslinks become more important. Because of this, *Mycobacterium tuberculosis* (Mtb) is more rapidly killed using a combination of drugs capable of PBP- and LDT- inhibition. Thus, knowledge about the single-cell distribution of drug targets can be exploited to more effectively treat this pathogen.

36

Introduction:

Peptidoglycan (PG) is an essential component of all bacterial cells (Vollmer, Blanot, & de Pedro, 2008a), and the target of many antibiotics. PG consists of linear glycan strands crosslinked by short peptides to form a continuous molecular cage surrounding the plasma membrane. This structure maintains cell shape and protects the plasma membrane from rupture. Our understanding of PG is largely derived from studies on laterally growing model rod-shaped bacteria like *Escherichia coli* and *Bacillus subtilis* (*Figure 1 - figure supplement 1A*). In these organisms, new PG is constructed along the

45 lateral side wall by the concerted effort of glycoslytransferases, which connect the glycan

46 of a new PG subunit to the existing mesh, and transpeptidases, which link peptide side

47 chains. An actin-like protein, MreB, positions this multi-protein complex along the short

48 axis of the cell so that glycan strands are inserted circumferentially, creating

49 discontinuous hoops of PG around the cell (Domínguez-Escobar et al., 2011; Garner et

50 al., 2011). This orientation of PG creates a mechanical anisotropy that is responsible for

51 rod shape (Hussain et al., 2018).

52 However, not all rod-shaped bacteria encode MreB. In fact, there are important

53 differences between model bacteria and Actinobacteria like mycobacteria, a genus of rod-

54 shaped bacteria that includes the major human pathogen *Mycobacterium tuberculosis*

55 (Mtb). In mycobacteria, new PG is inserted at the cell poles (at unequal amounts based

56 on pole age), rather than along the lateral walls (*Figure 1A*). Additionally, mycobacteria

57 are missing several factors, including MreB, that are important for cell elongation (Kieser

58 & Rubin, 2014). Furthermore, in *E. coli* and *B. subtilis* the vast majority (>90%) of the

59 peptide linkages are created by D,D-transpeptidases known as penicillin binding proteins

60 (PBPs) (Pisabarro, de Pedro, & Vázquez, 1985). PBPs, the targets of most β-lactams,

61 link the 4th amino acid of one peptide side chain to the 3rd amino acid of another, forming

62 4-3 crosslinks (*Figure 1- figure supplement 1B*). Peptide linkages can also be catalyzed

63 by L,D-transpeptidases (LDTs), which link peptide side chains by the 3rd amino acid

64 forming 3-3 linkages. In mycobacteria, these 3-3 crosslinks, are highly abundant,

65 accounting for ~60% of linkages (Kumar et al., 2012) (*Figure 1- figure supplement 1B*).

66 Because PG has been most well studied in bacteria where 3-3 crosslinks are rare, the

67 role of these linkages, and the enzymes that catalyze their formation, is poorly

68 understood.

69   Tuberculosis remains an enormous global health problem, in part, because

70 treating even drug susceptible disease is difficult. The standard regimen includes a

71 cocktail of four drugs given over six months. Treatment of drug-resistant Mtb is

72 substantially longer and includes combinations of up to seven drugs ("Global Tuberculosis

73 Report 2017," 2017). While some of the most important anti-mycobacterials target cell

74 wall synthesis, surprisingly, drugs that target PG are not part of the core treatment for

75 either drug-susceptible or drug-resistant disease. However, carbapenems, β-lactam

76 antibiotics that potently inhibit LDTs *in vitro*, are effective against drug resistant Mtb *in*

77 *vitro* and drug sensitive Mtb in patients (Diacon et al., 2016; Hugonnet, Tremblay, Boshoff,

78 Barry, & Blanchard, 2009).

79   But, why are LDTs important in mycobacteria? To explore this, we constructed

80 strains that lack the ability to form 3-3 crosslinks. We find that 3-3 crosslinks are formed

81 in maturing peptidoglycan and that they are necessary to stabilize the cell wall and

82 prevent lysis. Cells that lose the ability to synthesize 3-3 crosslinks have increased

83 dependence on 4-3 crosslinking. Thus, simultaneous inhibition of both processes results

84 in rapid cell death.

85

86 **Results:**

87 **Fluorescent D-amino acids are incorporated asymmetrically by LD-**

88 **transpeptidases**

4

89   PG uniquely contains D-amino acids, which can be labeled with fluorescent probes

90   (fluorescent D-amino acids, FDAAs) to visualize PG synthesis in live bacterial cells (Kuru

91   et al., 2012). When we incubated *M. smegmatis* (Msm), a non-pathogenic relative of Mtb,

92   with FDAAs for a short 2-minute pulse (< 2% of Msm's generation time) we observed

93   incorporation at both poles, the sites of new PG insertion in mycobacteria (*Figure 1A, B*)

94   (Aldridge et al., 2012). However, we also saw a gradient of fluorescence along the

95   sidewalls, extending from the old pole (the previously established growth pole) that fades

96   to a minimum at roughly mid-cell as it reaches the new pole (the pole formed at the last

97   cell division) (*Figure 1B*).

98   To identify the enzymes responsible for this unexpected pattern of lateral cell wall

99   FDAA incorporation, we performed a fluorescence-activated cell sorting (FACS)-based

100   transposon screen (*Figure 1C*). Briefly, we stained an Msm transposon library with FDAA

101   and repeatedly sorted the least fluorescent 12.5% of the population by FACS. After each

102   sort we regrew cells, extracted gDNA and used deep sequencing to map the location of

103   the transposons found in the low staining population.

104   From this screen, we identified three LDTs (*ldtA - MSMEG_3528, ldtB -*

105   *MSMEG_4745, ldtE - MSMEG_0233*) (*Figure 1D*) that were primarily responsible for

106   FDAA incorporation. Deleting these three LDTs significantly reduced FDAA incorporation

107   (*Figure 1- figure supplement 2A, B*). To further investigate the physiological role of LDTs,

108   we constructed a strain lacking all 6 LDTs (Δ*ldtAEBCGF*, hereafter ΔLDT). FDAA

109   incorporation and 3-3 crosslinking are both nearly abolished in ΔLDT cells and can be

110   partially restored by complementation with a single LDT (*ldtE*-mRFP; ΔLDT$_{comp}$) (*Figure*

111   *1E, F, Figure 1- figure supplement 2C, 3*). Thus, as might be the case in *Bdellovibrio*

112   (Kuru et al., 2017), FDAA incorporation in Msm is primarily LDT-dependent. LDTs have

113   previously been shown to exchange non-canonical D-amino acids onto PG tetrapeptides

114   in *Vibrio cholera* (Cava, de Pedro, Lam, Davis, & Waldor, 2011).

115

116   **LDT catalyzed 3-3 crosslinks are required for rod shape maintenance at aging cell**

117   **wall**

118   As deletion of a subset of LDTs in Msm produces morphologic changes (Sanders,

119   Wright, & Pavelka, 2014), we visualized ΔLDT cells by time-lapse microscopy. We

120   observed that a subpopulation of cells loses rod shape progressively over time, resulting

121   in localized spherical blebs (*Figure 2A - top, Figure 2 - figure supplement 1A, Figure 2 -*

122   *video 1*). Complemented cells are able to maintain rod shape (*Figure 2 - figure*

123   *supplement 1B*). We reasoned that localized loss of rod shape may occur for two reasons:

124   1) spatially-specific loss of cell wall integrity and/or 2) cell wall deformation due to

125   uncontrolled, local PG synthesis. If the first hypothesis were true, high osmolarity should

126   protect cells against forming blebs. Indeed, switching cells from iso- to high- osmolarity

127   prevented bleb formation over time (*Figure 2A, bottom, Figure 2- video 2*). To test the

128   second hypothesis, we stained ΔLDT cells with an amine-reactive dye, and observed

129   outgrowth of new, unstained material (*Figure 2B*). Blebs retained stain, indicating a lack

130   of new cell wall synthesis in the region. Collectively, these results indicate that 3-3

131   crosslinks are required to counteract turgor pressure and maintain the rod shape of

132   mycobacteria. This led us to hypothesize that bleb formation is a result of a local defect

133   in cell wall rigidity.

134   To directly measure cell wall rigidity, we used atomic force microscopy (AFM) on

135   live ΔLDT and WT cells. We measured the rigidity of cells in relation to their height.

136   Generally, WT cells are stiffer than ΔLDT cells (*Figure 2D*). Blebs in ΔLDT cells can be

137   identified by a sharp increase in height (*Figure 2E, pink shaded*). Since circumferential

138   stress of the rod measured by AFM is proportional to the radius of the cell, and inversely

139   proportional to the thickness of the cell wall (an immeasurable quantity by AFM), we used

140   cell height, a proxy for radius, to normalize the stiffness measurement. We found that

141   stiffness drops in the area of blebs (*Figure 2E, pink shaded*).

142   Why does loss of rod shape occur locally and only in a subpopulation of cells?

143   Mycobacterial polar growth and division results in daughter cells with phenotypic

144   differences (Aldridge et al., 2012). For example, the oldest cell wall is specifically inherited

145   by the new pole daughter (*Figure 2- supplement 2A*, (Aldridge et al., 2012)). We

146   hypothesized that the loss of rod shape might occur in specific progeny generated by cell

147   division. Indeed, the daughter which inherited the new pole from the previous round of

148   division, and the oldest cell wall, consistently lost rod shape over time, while the old pole

149   daughter maintained rod shape (*Figure 2C, Figure 2- supplement 2B*). In addition, blebs

150   localized to the oldest cell wall (*Figure 2B*), as visualized by pulse-chase labeling of the

151   cell wall. Thus, 3-3 crosslinking is likely occurring in the oldest cell wall, which is non-

152   uniformly distributed along a single cell and in the population via asymmetric polar growth

153   and division. Taken together, these data suggest that LDTs act locally to reinforce aging

154   PG and to maintain rod shape in a subpopulation of Msm cells - specifically, new pole

155   daughters (*Figure 2F*).

156

Mycobacteria are hypersensitive to PBP inactivation in the absence of LDTs

Our observations lead to the following model (*Figure 6A*): PBP-catalyzed 4-3 crosslinks are formed at the poles where new PG is inserted and where pentapeptide substrates reside. These newly synthesized 4-3 crosslinks are then gradually cleaved (by D,D-endopeptidases) as PG ages and moves toward the middle of the cell, leaving tetrapeptide substrates for LDTs to create 3-3 crosslinks. This is consistent with the FDAA incorporation pattern, which reflects the abundance of tetrapeptide substrates available for LDT exchange. Specifically, there are more available tetrapeptides near the poles and fewer near mid-cell, the site of older PG (*Figure 1F*). In the absence of LDTs to catalyze 3-3 crosslinks, old cell wall loses integrity and turgor pressure causes bleb formation.

This model predicts that ΔLDT cells should be even more dependent on 4-3 crosslinking than wild type cells. To test this hypothesis, we used TnSeq (Long et al., 2015) to identify genes required for growth in cells lacking LDTs (*Figure 3A*). We found that mutants of two PBPs, *pbpA (MSMEG_0031c)* and *ponA2 (MSMEG_6201)*, were recovered at significantly lower frequencies in ΔLDT cells (*Figure 3B*). Likewise, using allele swapping (Kieser, Boutte, et al., 2015b) (*Figure 3C, Figure 3- figure supplement 1A*), a technique that tests the ability of various alleles to support viability, we found that the transpeptidase (TP) activity of PonA1, which is non-essential in WT cells (Kieser, Boutte, et al., 2015b), becomes essential in ΔLDT cells (*Figure 3D*). Thus, cells that lack 3-3 crosslinks are more dependent on 4-3 crosslinking enzymes.

Peptidoglycan synthesizing enzymes localize to differentially aged cell wall

179   Given our model, we hypothesized that enzymes catalyzing and processing

180   different types of crosslinks should be differentially localized along the length of the cell.

181   Specifically, we postulated that 4-3 crosslinking PBPs would localize at sites of new PG,

182   while 4-3 cleaving D,D-endopeptidases and 3-3 crosslinking LDTs would localize to sites

183   of older PG. To test whether 3-3 and 4-3 crosslinking enzymes localize differently, we

184   visualized fluorescent fusions of a PBP (PonA1), and an LDT (LdtE), (*Figure 4A*). We

185   found that PonA1-RFP largely localized to the old pole, where new PG is inserted (*Figure*

186   *4A, B, Figure 4 - video 1*). LdtE-mRFP localized farther from the poles, the sites of older

187   PG (*Figure 4A, B, Figure 4 - video 2*). Thus, enzymes responsible for 4-3 and 3-3

188   crosslinks exhibit distinctive subcellular localizations, consistent with the model that they

189   act on differentially aged PG.

190   We next sought to localize a D,D-endopeptidase. As no D,D-endopeptidase has

191   been clearly identified in mycobacteria, we used HHPRED (Zimmermann et al., 2017) to

192   find candidates. By homology to the *E. coli* protein AmpH, an enzyme with both D,D-

193   carboxy- and endopeptidase activity (González-Leiza, de Pedro, & Ayala, 2011), we

194   identified   DacB2   (MSMEG_2433),   a   protein   previously   shown   to   have   D,D-

195   carboxypeptidase activity in Msm (Bansal et al., 2015), as a candidate to also harbor D,D-

196   endopeptidase capability. We expressed and purified DacB2 and found that it, like AmpH,

197   had   both   D,D-carboxypeptidase   and   D,D-endopeptidase   activity   on   peptidoglycan

198   substrates generated *in vitro* (*Figure 4C, Figure 4- figure supplement 1A-C*). Consistent

199   with our model, DacB2-mRFP localized closer to LDT-mRFP, farther from the poles, at

200   sites of older PG (*Figure 4A, B, Figure 4 – video 3*). Thus, bleb formation may result from

201   unchecked D,D-endopeptidase activity in ΔLDT cells.

Drugs targeting both PBPs and LDTs synergize to kill Mtb

The importance of 3-3 crosslinks in mycobacteria suggests a unique vulnerability. While Mtb can be killed by most non-carbapenem (N-C) β-lactams like penicillins, which largely target the PBPs, carbapenem β-lactams, which target both PBPs and LDTs (Mainardi et al., 2007; Papp-Wallace, Endimiani, Taracila, & Bonomo, 2011) are also effective against Mtb (Diacon et al., 2016; Hugonnet et al., 2009). As has been previously proposed (Gonzalo & Drobniewski, 2013; Gupta et al., 2010; Mainardi et al., 2007), our data suggest that more rapid killing of Mtb could be achieved with drug combinations that target both PBPs and LDTs (*Figure 5A*). In fact, we find that the combination of amoxicillin (a penicillin) and meropenem (a carbapenem), exhibits synergism in minimal inhibitory concentration (Σ Fractional Inhibitory Concentration < 0.5 ("Synergism Testing: Broth Microdilution Checkerboard and Broth Macrodilution Methods," 2016), *Figure 5B, Figure 5- figure supplement 1A,B*). We also see that this combination leads to more rapid killing of Mtb *in vitro* (*Figure 5B, Figure 5- figure supplement 2A*) (Andreu, Fletcher, Krishnan, Wiles, & Robertson, 2012).

Discussion:

The success of antibiotics that target PG, like β-lactams, has led to decades of research of this critical bacterial polymer. Recently developed fluorescent probes (FDAAs) of PG synthesis have been used extensively to study PG-synthesis in live cells of numerous bacterial species. Intriguingly, these probes can be incorporated through diverse pathways in different bacteria and thus, their pattern can mark distinct processes (Kuru et al., 2012). Here, we find that, in mycobacteria, FDAA incorporation is primarily

225 LDT-dependent. FDAA incorporation in Msm shows an unusual gradient pattern (Botella

226 et al., 2017), suggesting an asymmetric distribution of tetrapeptide substrate for the LDT-

227 dependent exchange reaction. In addition to their ability to exchange D-amino acids onto

228 tetrapeptides, LDTs also catalyze non-canonical 3-3 crosslinks.

229 LDT-catalyzed crosslinks are rare in model rod-shaped bacteria like *E.coli* and *B.*

230 *subtilis* but, are abundant in polar growing bacteria like mycobacteria, *Agrobacterium*

231 *tumefaciens* and *Sinorhizobium meliloti* (Brown et al., 2012; Cameron, Zupan, &

232 Zambryski, 2015; Kumar et al., 2012; Lavollay et al., 2008; Pisabarro et al., 1985)*. Here,

233 we find that Msm cells lacking 3-3 crosslinks cannot maintain rod shape at sites of aging

234 cell wall. PBP-catalyzed 4-3 crosslinks appear able to maintain rod shape near the poles,

235 the sites of newer cell wall (*Figure 6A*). Over time, older cell wall moves towards the

236 middle of the cell, loses structural stability, and begins to bleb. The gradual manner in

237 which rod shape is lost suggests that cell wall processing must occur to de-stabilize this

238 portion of the rod. Consistent with this idea, we find that an enzyme that cleaves 4-3

239 crosslinks, DacB2, also localizes to sites of old cell wall.

240 Why would Msm cells create 4-3 crosslinks to eventually cleave them? There are

241 many possibilities. For example, perhaps in the absence of lateral cell wall synthesis, the

242 creation of substrate for LDTs through the destruction of 4-3 crosslinks allows the cell to

243 engage the PG along the lateral cell body. This could be important for altering the

244 thickness of the PG layer or anchoring it to the membrane at sites of otherwise "inert" cell

245 wall. Additionally, it may be that as PG ages, it is being manicured for septal synthesis.

246 Supporting this idea, we find that the localization patterns of PonA1, LdtE and DacB2,

247 and FDAA all have local minima at mid-cell closer to the new pole, the asymmetric site of

248 division in mycobacteria (Aldridge et al., 2012; Dhar, Bousbaine, Wakamoto, McKinney,

249 & Santi, 2013; Eskandarian et al., 2017). This lack of localization suggests a lack of penta-

250 and tetra- peptide substrates, implying that that this region of the cell more abundantly

251 crosslinked, as crosslinking utilizes these peptide species. Mycobacteria are missing

252 known molecular septal placement mechanisms like the Noc and the Min system (Hett &

253 Rubin, 2008). Could 3-3 crosslinking be a signal for septal placement? Indeed, the major

254 septal PG hydrolase is RipA, a D,L-endopeptidase which cleaves the bond between the

255 second and third amino acid of PG side chains, a substrate available on 3-3 crosslinked

256 material (Böth, Schneider, & Schnell, 2011; Vollmer, Joris, Charlier, & Foster, 2008b).

257 Thus, it is intriguing to speculate that 3-3 crosslinks could be important for localizing cell

258 division machinery.

259   In well-studied rod-shaped bacteria like *E.coli* and *B. subtilis*, shape is maintained

260 by MreB-directed PG synthesis along the lateral cell body (Garner et al., 2011; Hussain

261 et al., 2018; Ursell et al., 2014). On the other hand, mycobacteria maintain shape in the

262 absence of an obvious MreB homolog, and in the absence of lateral cell wall elongation.

263 Furthermore, in contrast to lateral-elongating bacteria, in which new and old cell wall are

264 constantly intermingled during growth, polar growth segregates new and old cell wall

265 (*Figure 6B*). We find that mycobacteria appear to utilize 3-3 crosslinks at asymmetrically

266 distributed aging cell wall to provide stability along the lateral body, something that may

267 not be required in the presence of MreB-directed PG synthesis.

268   New drug combinations for TB are desperately needed. Indeed, there has been a

269 renewed interest in repurposing FDA-approved drugs for TB treatment (Diacon et al.,

270 2016). Our results suggest that a better understanding of the localization and distribution

271 of drug targets in single cells may lead to rational predictions of drug combinations.

272 Indeed, we find that enzymes which do very similar chemistry – PG crosslinking – are

273 distributed differentially in a single cell and across the population. In the absence of 3-3

274 crosslinks, 4-3 crosslinks become more important for cell viability. These data predict that

275 a drug combination which inhibits both PBPs and LDTs will work synergistically to more

276 quickly kill Mtb, a prediction we verified *in vitro*. Interestingly, meropenem combined with

277 amoxicillin/clavulanate resulted in early clearance of Mtb from patient sputum (Diacon et

278 al., 2016). In fact, the combination might be key to accelerated killing of Mtb (Gonzalo &
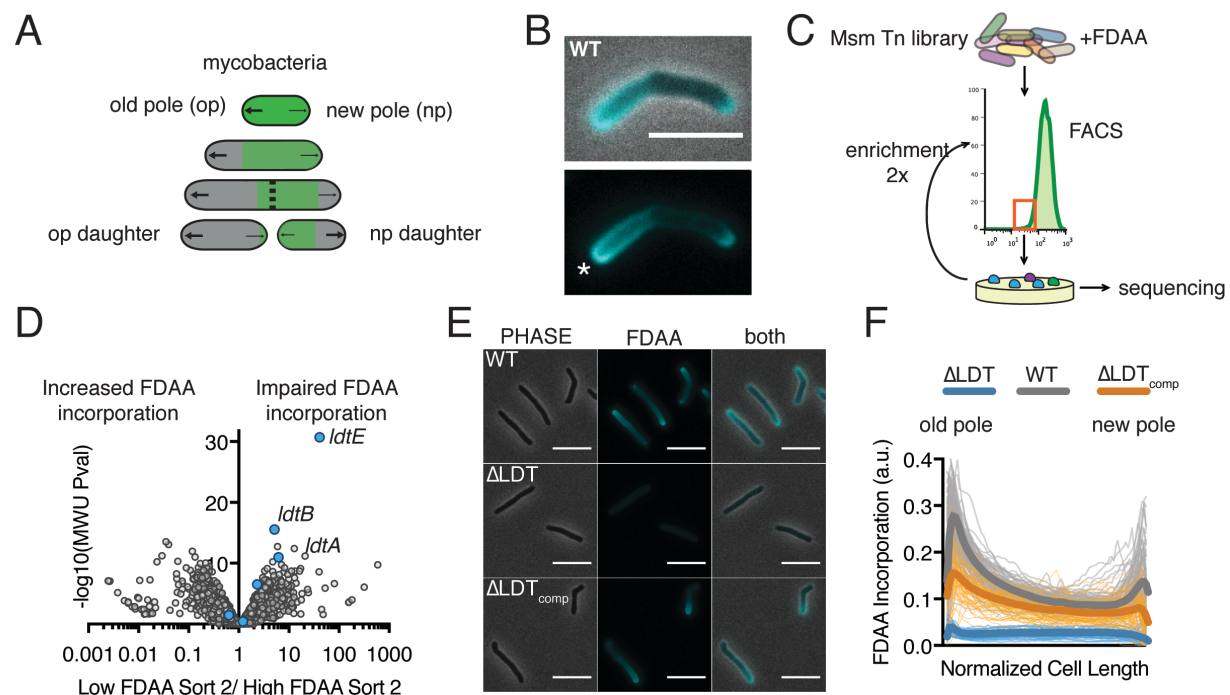
279 Drobniewski, 2013).

280

300

Figure 1: FDAAs are incorporated asymmetrically by LD-transpeptidases. (A) Schematic of mycobacterial asymmetric polar growth. Green, old cell wall; grey, new material; dotted line, septum; large arrows, old pole growth; small arrows, new pole growth. **(B)** FDAA incorporation in log-phase WT Msm cell after 2-minute incubation. Scale bar=5μm. Old pole marked with (*). **(C)** Schematic of Fluorescence Activated Cell Sorting (FACS)-based FDAA transposon library enrichment. An Msm transposon (Tn) library was stained with FDAAs, the dimmest and brightest cells were sorted, grown, sorted again to enrich for transposon mutants that are unable or enhanced for FDAA incorporation. **(D)** Results from 1C screen. For each gene, the contribution to low or high staining population was calculated from transposon reads per gene. Plotted is the ratio of the population contribution from the second sort of low FDAA staining (L2) over the second sort of high FDAA staining (H2) cells compared to the Mann-Whitney *U* P-value. **(E)** Representative image of FDAA incorporation in log-phase WT, ΔLDT and ΔLDT_comp cells. Scale bar= 5μm. **(F)** Profiles of FDAA incorporation in log-phase WT (N=98), ΔLDT (N=40), and ΔLDT_comp (N=77) cells. Thick lines represent mean incorporation profile, thin lines are FDAA incorporation in single cells.
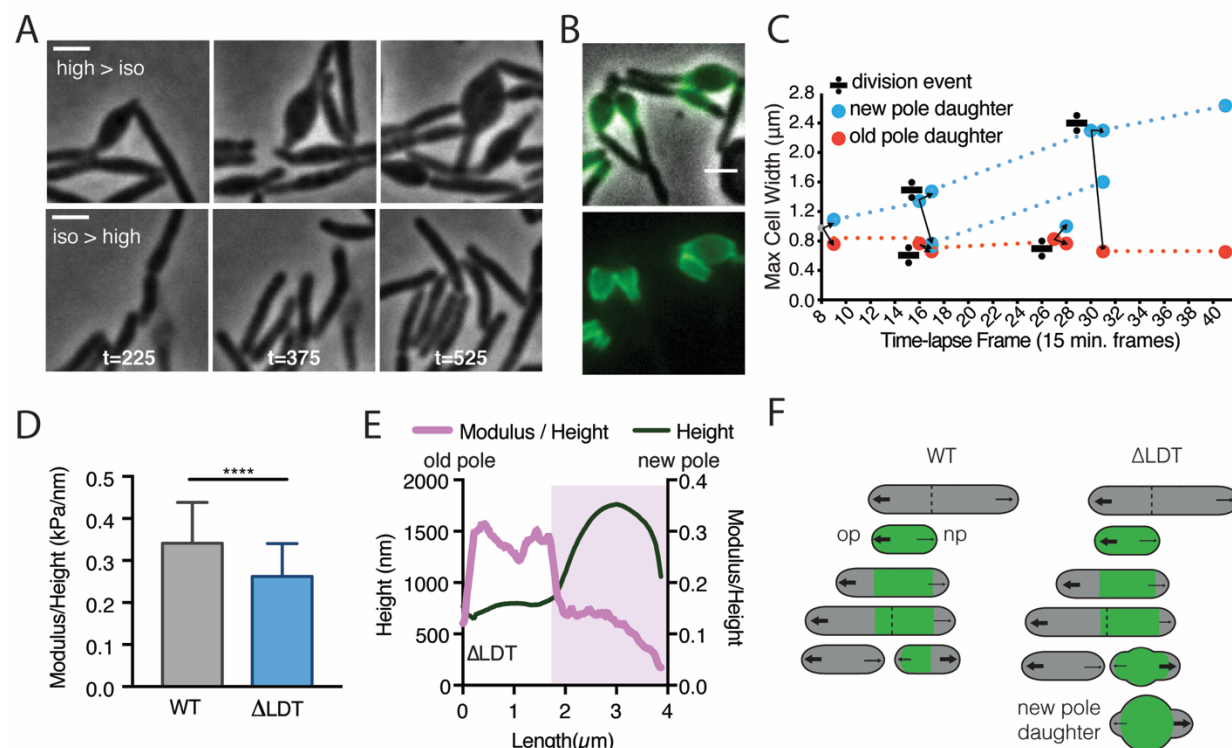
321
322
323 **Figure 2: LDT catalyzed 3-3 crosslinks are required for rod shape maintenance at**
324 **aging cell wall. (A)** Msm ΔLDT time-lapse microscopy of cells switched from high- to iso-
325 (top) osmolar media, or iso- to high osmolar media (bottom). (high=7H9+150mM sorbitol;
326 iso=7H9). t= time in minutes post osmolarity switch. **(B)** ΔLDT cells were stained with
327 Alexa 488 NHS-ester (green) to mark existing cell wall, washed, and visualized after
328 outgrowth (unstained material). A, B scale bar=2μm. **(C)** Maximum cell width of ΔLDT cell
329 lineages over time. Width of new pole daughters = blue circle; width of old pole daughters
330 = orange circle. Division signs denote a division event. At each division, there are two
331 arrows from the dividing cell leading to the resulting new and old pole daughter cell widths
332 (blue and orange respectively). **(D)** Mean stiffness of WT (N=73) and ΔLDT (N=47) Msm
333 cells as measured by atomic force microscopy. Mann-Whitney U P-Value **** < 0.0001.
334 **(E)** Representative profile of cell height and height-normalized stiffness (modulus/height)
335 in a single ΔLDT cell. Pink shaded portion highlights location of a bleb. **(F)** Model of rod
336 shape loss in old cell wall of ΔLDT cells compared to WT. Green portions of the cell
337 represents old cell wall; grey portion represents new cell wall. The larger arrows indicate
338 more growth from the old pole, while smaller arrows show less relative growth from the
339 new pole. Dotted lines represent septa. op= old pole, np=new pole.
340
341
342
343
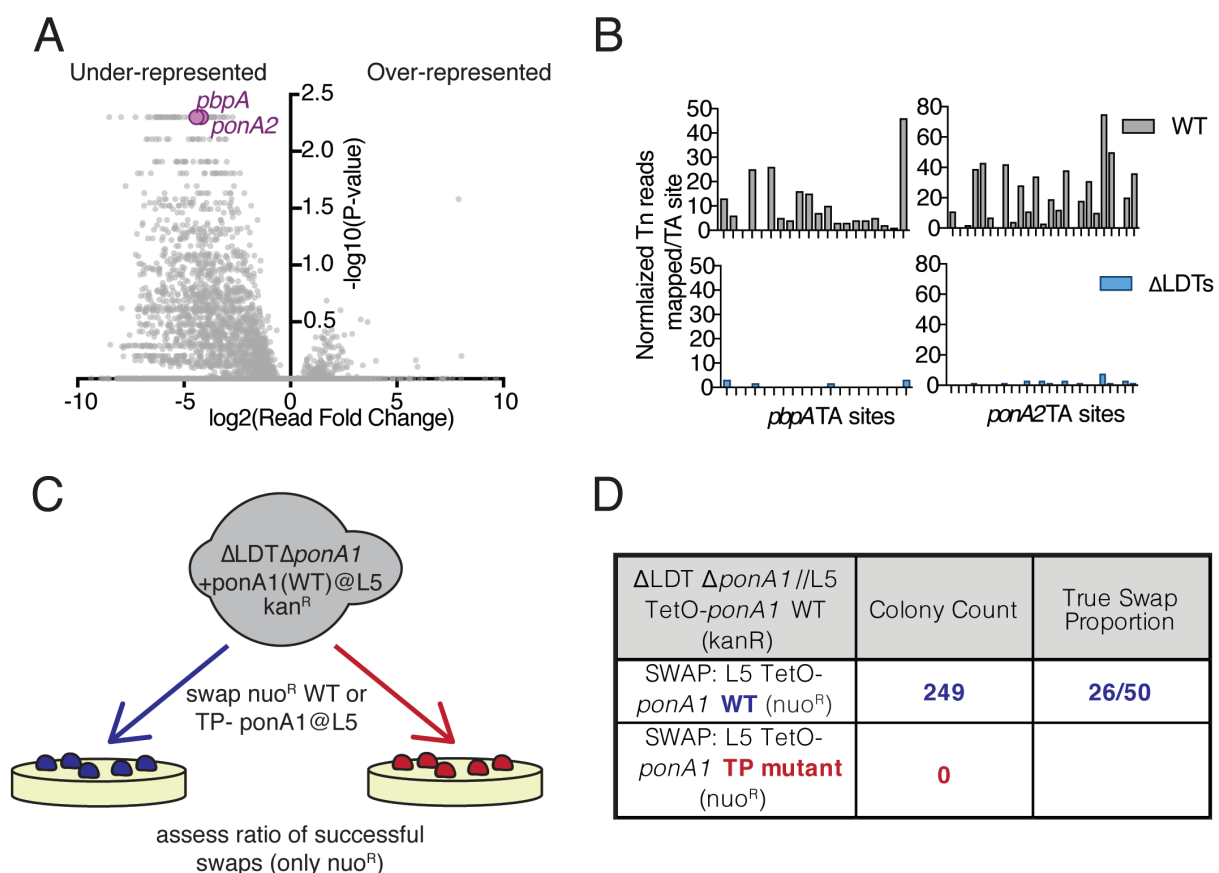
Figure 3: Mycobacteria are hypersensitive to PBP inactivation in the absence of LDTs. (A) Fold change in the number of reads for transposon insertion counts in ΔLDT cells compared to WT Msm. P-value is derived from a rank sum test (DeJesus, Ambadipudi, Baker, Sassetti, & Ioerger, 2015). **(B)** Transposon insertions per TA dinucleotide in *pbpA* and *ponA2* in WT (grey) and ΔLDT (blue) cells. **(C)** Schematic of L5 allele swapping experiment. Adapted from (Kieser, Boutte, et al., 2015b). **(D)** Results of WT or transpeptidase null *ponA1* allele swapping experiment in ΔLDT cells.
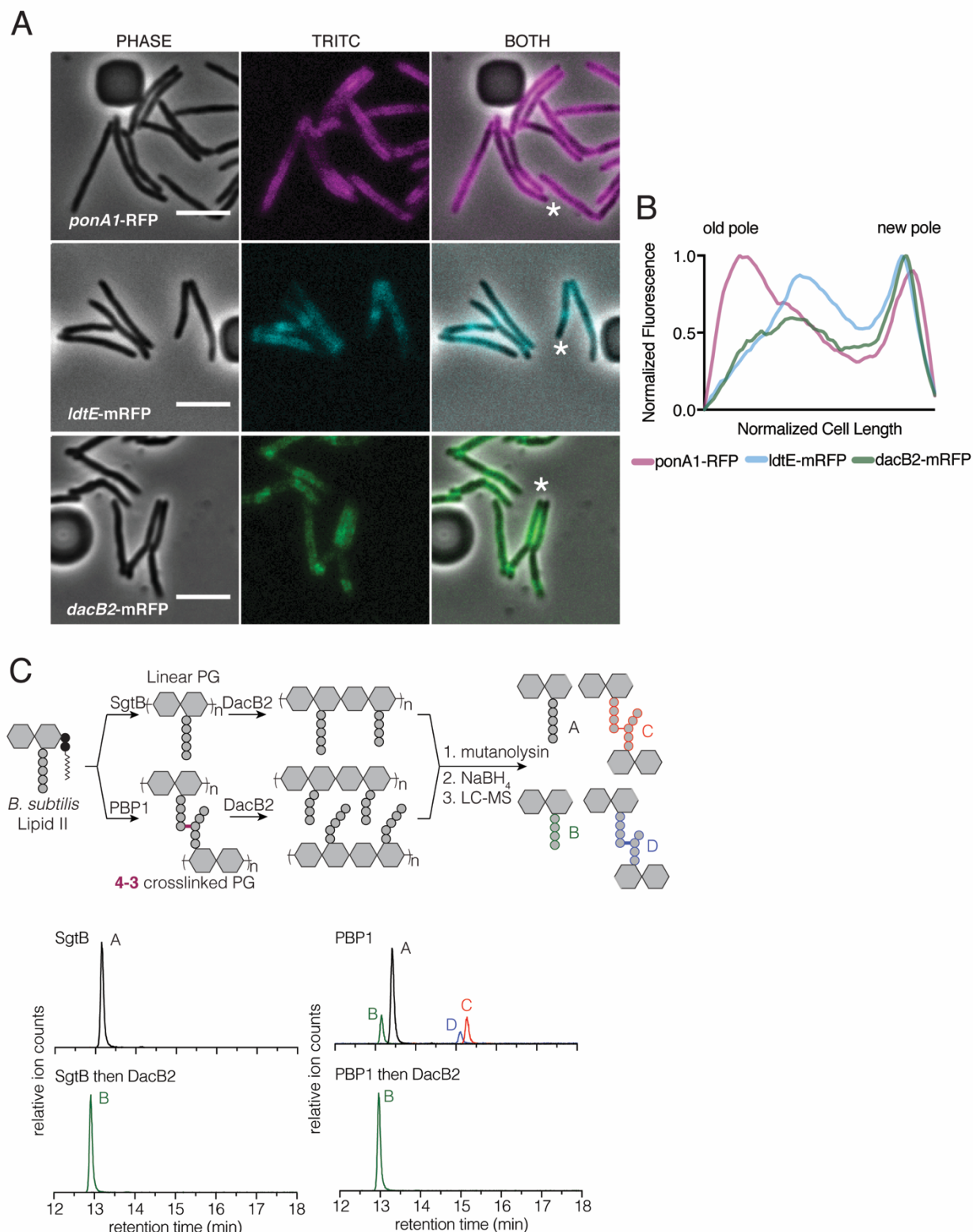
Figure 4: Peptidoglycan synthesizing enzymes localize to differentially aged cell wall. (A) Representative fluorescence images of PonA1-RFP (magenta), LdtE-mRFP (cyan), and DacB2-mRFP (green). Scale bars=5µm. **(B)** Average PonA1-RFP (N=24),

358   LdtE-mRFP (N=23) or DacB2-mRFP (N=23) distribution in cells before division. **(C)**
359   Schematic of the *in vitro* experiment to test D,D-carboxy- and D,D-endopeptidase activity
360   of DacB2. Lipid II extracted from *B. subtilis* is first polymerized into linear (using SgtB) or
361   crosslinked (using *B. subtilis* PBP1) peptidoglycan and then reacted with DacB2. The
362   reaction products are analyzed by LC-MS. **(below)** Extracted ion chromatograms of the
363   reaction products produced by incubation of DacB2 with peptidoglycan substrates.
364
365
366

367
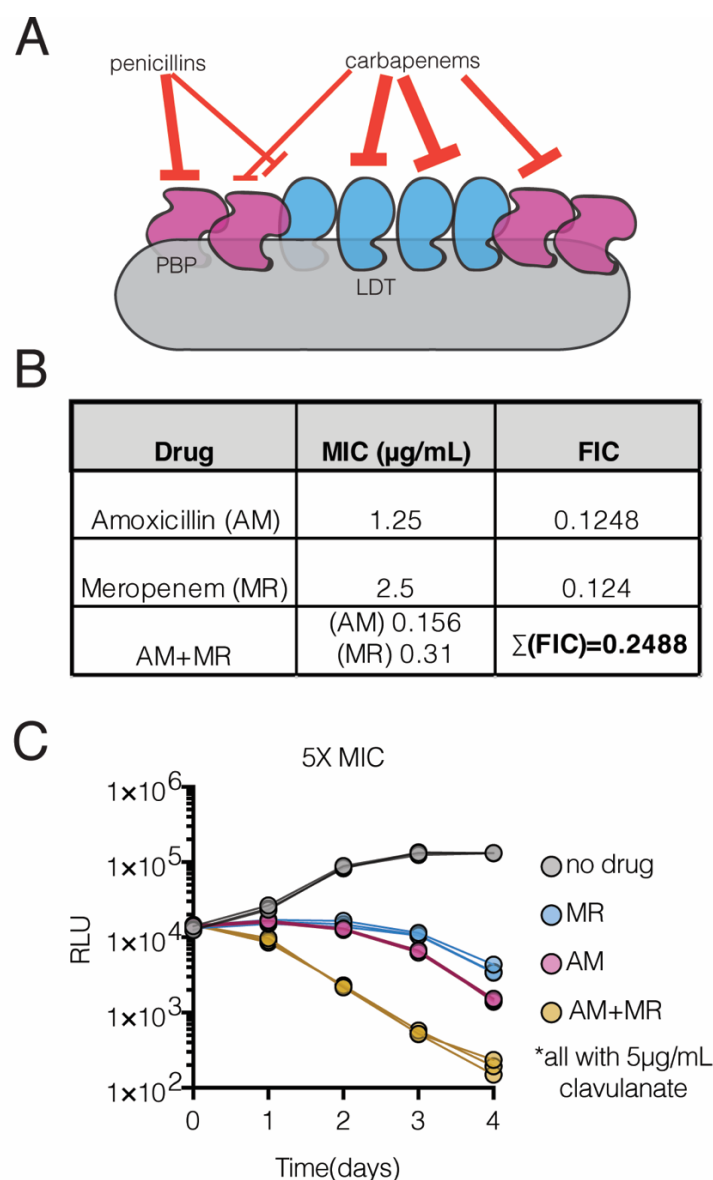
Figure 5: Drugs targeting both PBPs and LDTs synergize to kill Mtb. **(A)** Schematic of synergistic targeting of PBPs and LDTs by pencillin and carbapenem β-lactams. **(B)** Minimum inhibitory concentration (MIC) of amoxicillin, meropenem, or the combination, in *M. tuberculosis*. FIC (fractional inhibitory concentration) = MIC of drug in combination/MIC of drug alone. Synergy is defined as ∑ FIC<=0.5 ("Synergism Testing: Broth Microdilution Checkerboard and Broth Macrodilution Methods," 2016). **(C)** Killing dynamics of *M. tuberculosis* (expressing the *luxABCDE* operon from *Photorhabdus luminescens* (Andreu et al., 2010)) measured via luciferase production (RLU=relative light units). 5X MIC Amoxicillin (AM) (3.125 µg/mL); 5X MIC Meropenem (MR) (6.25 µg/mL); Amoxicillin+Meropenem 3.125 µg/mL AM; 6.25 µg/mL MR). Biological triplicate are plotted. All drugs were used in combination with 5µg/mL clavulanate.

379
380
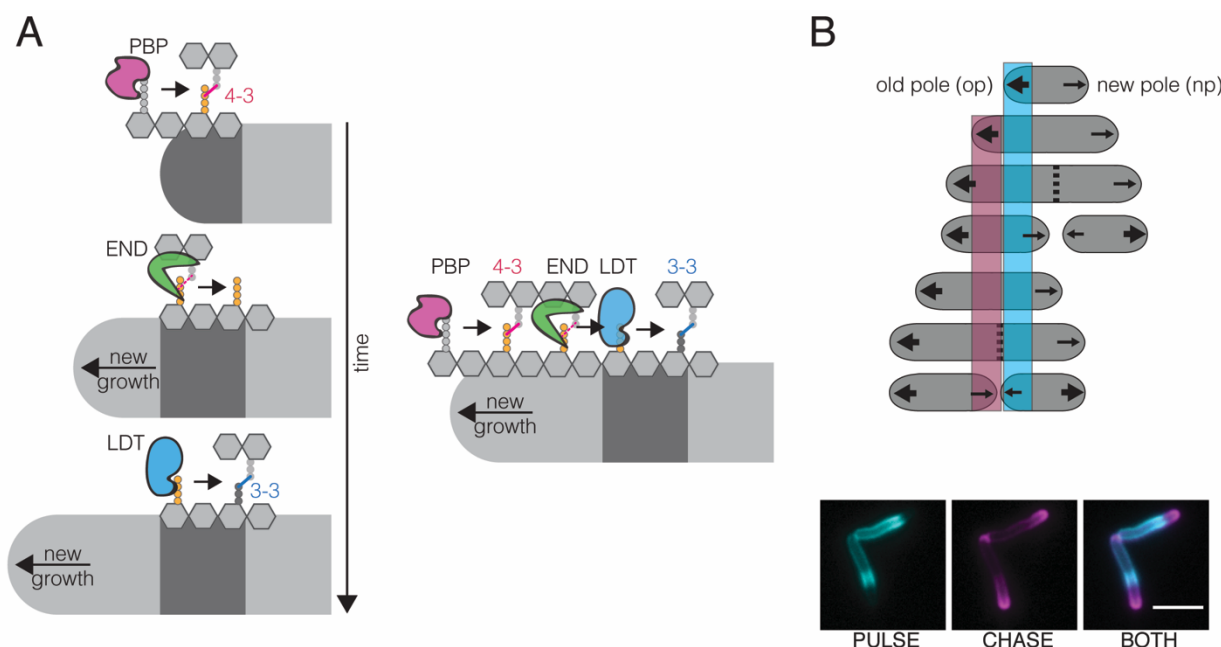
Figure 6: Model for PG enzyme and substrate distribution as governed by polar growth and PG segregation by age. (A) A model for PG age, PG enzyme and crosslink segregation via polar growth in mycobacteria. **(B)** Schematic of PG segregation by age (top). 2-minute FDAA pulse (cyan), 45-minute outgrowth, followed by 2-minute FDAA chase (magenta) in WT Msm cells (bottom). Newest cell wall (magenta), older cell wall (cyan). Scale bar=5µm

387

388 **Supplementary Materials**

389

390 **Materials and Methods**

391 Bacterial strains and culture conditions

392 Unless otherwise stated, *Mycobacterium smegmatis* (mc²155) was grown shaking at

393 37°C in liquid 7H9 media consisting of Middlebrook 7H9 salts with 0.2% glycerol,

394 0.85g/L NaCl, ADC (5g/L albumin, 2g/L dextrose, 0.003g/L catalase), and 0.05% Tween

395 80 and plated on LB agar. *Mycobacterium tuberculosis* (H37Rv) was grown in liquid

396 7H9 with OADC (oleic acid, albumin, dextrose, catalase) with 0.2% glycerol and 0.05%

397 Tween 80. Antibiotic selection for *M. smegmatis* and *M. tuberculosis* were done at the

398 following concentrations in broth and on agar: 25μg/mL kanamycin, 50μg/mL

399 hygromycin, 20μg/mL zeocin and 20μg/mL nourseothricin and, twice those

400 concentrations for cloning in *Escherichia coli* (TOP10, XL1-Blue and DH5α).

401

402 Strain construction

403 *M. smegmatis* mc²155 mutants lacking *ldtABECFG (*ΔLDT) was constructed using

404 recombineering to replace endogenous copies with zeocin or hygromycin resistance

405 cassettes flanked by lox sites as previously described (Boutte et al., 2016). Briefly, 500

406 base pairs of upstream and downstream sequence surrounding the gene of interest

407 were amplified via PCR (KOD Xtreme^{TM} Hot Start DNA polymerase (EMD Millipore,

408 Billerica, MA)). These flanking regions were amplified with overlaps to either a zeocin or

409 hygromycin resistance cassette flanked by loxP sites and these pieces were assembled

410 into a deletion construct via isothermal assembly (Gibson et al., 2009). Each deletion

411   cassette was transformed into Msm expressing inducible copies of RecET for

412   recombination (Murphy, Papavinasasundaram, & Sassetti, 2015). Once deletions were

413   verified by PCR using and sequencing, the antibiotic resistance cassettes were

414   removed by the expression of Cre recombinase. The order of deletion construction in

415   the ΔLDT strain was as follows (where arrows represent transformation of a Cre-

416   recombinase plasmid, followed by curing of the Cre-recombinase plasmid as it contains

417   the *sacB* gene for sucrose counter selection on LB supplemented with 10% sucrose,

418   and strain names are listed in parenthesis). This resulted in the removal of antibiotic

419   cassettes flanked by loxP sites:

420   1) mc^{2}155Δ*ldtA*:: zeo^R (KB103)→ mc^{2}155Δ*ldtA*::loxP (KB134)

421   2) mc^{2}155Δ*ldtA::loxP* + Δ*ldtE*:: zeo^R (KB156)

422   3) mc^{2}155Δ*ldtA::loxP* Δ*ldtE*:: zeo^R + Δ*ldtB*:: hyg^R (KB200) → mc^{2}155Δ*ldtA::loxP*

423   Δ*ldtE*::loxP Δ*ldtB*::loxP (KB207)

424   4) mc^{2}155Δ*ldtA::loxP* Δ*ldtE*::loxP Δ*ldtB*::loxP + Δ*ldtC*:: hyg^R (KB209)

425   5)mc^{2}155Δ*ldtA::loxP* Δ*ldtE*::loxP Δ*ldtB*::loxP Δ*ldtC*:: hyg^R Δ*ldtG*:: zeo^R (KB222)→

426   mc^{2}155Δ*ldtA::*loxP Δ*ldtE*::loxP Δ*ldtB*::loxP Δ*ldtC*:: loxP Δ*ldtG*:: loxP (KB241)

427   6) mc^{2}155Δ*ldtA::*loxP Δ*ldtE*::loxP Δ*ldtB*::loxP Δ*ldtC*:: loxP Δ*ldtG*:: loxP Δ*ldtF*:: hyg^R

428   (KB303 referred to as ΔLDT) .

429

430   *M. tuberculosis* H37Rv was transformed with a vector expressing the codon optimized

431   *Photorhabdus luminescens luxABCDE* operon (pMV306hsp+LuxG13 –Addgene

432   #26161)(Andreu et al., 2010). This strain is referred to as Mtb Lux.

433

434 Refer to Supplemental Table 1 for oligonucleotides, and Supplemental Table 2 for a

435 complete strain list.

436

437 ΔLDT complementation plasmid construction

438 To complement ΔLDT we placed a copy of *ldtE* (*MSMEG_0233*) under the constitutive

439 TetO promoter (a UV15 derivative within a pMC1s plasmid that is inducible with

440 anhydrous tetracycline in the presence of a tet-repressor TetR, which the ΔLDT$_{comp}$

441 strain lacks (Kieser, Boutte, et al., 2015b)) on vector that integrates at the L5 phage

442 integration site of the chromosome of the ΔLDT strain (the vector is marked with

443 kanamycin resistance). A glycine, glycine, serine linker was cloned between *ldtE* and

444 mRFP in this complementation construct.

445

446 PonA1 transpeptidase essentiality L5 allele swapping

447 To test essentiality of transpeptidation by PonA1 in the ΔLDT cells, L5 allele swapping

448 as described in (Kieser, Boutte, et al., 2015b) was performed. The plasmids used in

449 this experiment were previously published in (Kieser, Boutte, et al., 2015b). Briefly, a

450 wild-type copy of PonA1 (TetO driven expression, L5 integrating and kanamycin

451 marked) was transformed into ΔLDT. Then, the endogenous copy of *ponA1* was

452 replaced with zeocin using the above mentioned recombineering technique (amplifying

453 the construct from a previously published deletion mutation of *ponA1*(Kieser, Boutte, et

454 al., 2015b)). Swapping efficiency of either wildtype or transpeptidase mutant PonA1

455   marked with nourseothricin was tested with a transformation into ΔLDT//L5-TetO-ponA1

456   (WT)-kanamycin.

457

458   *M. tuberculosis* minimum inhibitory concentration (MIC) determination

459   Mtb Lux was grown to log phase and diluted to an OD_{600}=0.006 in each well of non-

460   treated 96 well plates (Genessee Scientific) containing 100μL of meropenem (Sigma

461   Aldrich) and/or amoxicillin (Sigma Aldrich) diluted in 7H9+OADC+5μg/mL clavulanate

462   (Sigma Aldrich). Cells were incubated in drug at 37°C shaking for 7 days, 0.002%

463   resazurin (Sigma Aldrich) was added to each well, and the plates were incubated for 24

464   hours before MICs were determined. Pink wells signify metabolic activity and blue

465   signify no metabolic activity. (Kieser, Baranowski, et al., 2015a) Checkerboard MIC

466   plates and fractional inhibitory concentrations were calculated as described in

467   ("Synergism Testing: Broth Microdilution Checkerboard and Broth Macrodilution

468   Methods," 2016).

469

470   *M. tuberculosis* drug killing assays

471   Mtb Lux was grown to log phase (kanamycin 25μg/mL) and diluted in 30mL inkwells

472   (Corning Lifesciences) to an OD_{600}=0.05 in 7H9+OADC+5μg/mL clavulanate with

473   varying concentrations of amoxicillin, meropenem, or both. 100μL of these cultures

474   were pipetted in duplicate into a white 96-well polystyrene plate (Greiner Bio-One) and

475   luminescence was read in a Synergy H1 microplate reader from BioTek Instrumenmts,

476   Inc. using the Gen5 Software (2.02.11 Installation version). The correlation between

477   relative light units (RLU) and colony forming units (CFU) is shown in Msm in Figure 5 –

478   figure supplement 2.

479

480   <u>Fluorescent D-amino acid labeling</u>

481   NADA (3-[7-nitrobenzofurazan]-carboxamide-D-alanine), HADA (3-[7-hydroxycoumarin]-

482   carboxamide-D-alanine) and TADA (3-[5-carboxytetramethylrhodamine]-carboxamide-

483   D-alanine) were synthesized by Tocris following the published procotol (Kuru, Tekkam,

484   Hall, Brun, & Van Nieuwenhze, 2014). To 1mL of exponentially growing cells 0.1mM of

485   FDAA final was added and incubated for 2 minutes before washing in 7H9 twice. For

486   still imaging, after the second wash, cells were fixed in 7H9 + 1% paraformaldehyde

487   before imaging. For pulse chase experiments, cells were stained, washed with 7H9 and

488   allowed to grow out for 40 minutes before being stained with a second dye and imaged.

489   <u>Flow cytometry</u>

490   An *M. smegmatis* transposon library was grown to mid-log phase, and stained with 2

491   µg/mL NADA for 2 minutes. Cells were centrifuged and half of the supernatant was

492   discarded. The pellet was resuspended in the remaining supernatant, passed through a

493   10µm filter and taken to be sorted (FACSAria; Excitation: 488nm; Emission filter:

494   530/30). Two bins were drawn at the lowest and highest staining end of the population,

495   representing 12.5% of the population. 600,000 cells from these bins were sorted into

496   7H9 medium. Half of this was directly plated onto LB agar supplemented with

497   kanamycin to select for cells harboring the transposon. The remaining 300,000 cells

498   were grown out in 7H9 to log phase, stained with FDAA and sorted again to enrich the

499   populations.

500

501 <u>Transposon sequencing, mapping and FDAA flow cytometry enrichment analysis.</u>

502 Genomic DNA (gDNA) was harvested from the sorted transposon library colonies and

503 transposon-gDNA junction libraries were constructed and sequenced using the Illumina

504 Hi-Seq platform (Long et al., 2015). Reads were mapped on the *M. smegmatis* genome,

505 tallied and reads at each TA site for the bins (low/high incorporating sort 1 and 2) were

506 imported into MATLAB and processed by a custom scripts as described in (Rego,

507 Audette, & Rubin, 2017).

508

509 <u>Microscopy</u>

510 Both still imaging and time lapse microscopy were performed on an inverted Nikon TI-E

511 microscope at 60x magnification. Time lapse was done using a CellASIC (B04A plate)

512 with constant liquid 7H9 flow in a 37°C chamber. For turgor experiment (*Figure 2A*),

513 cells were grown in either 7H9 or 7H9 500mM sorbitol overnight, and then switched to

514 either 7H9 with 150mM sorbitol (high osmolar) or to 7H9 alone (iso-osmolar).

515

516 <u>Atomic force microscopy</u>

517 AFM experimentation was conducted as previously(Eskandarian et al., 2017). In short,

518 polydimethylsiloxane (PDMS) – coated coverslips were prepared by spin-coating a

519 mixture of PDMS at a ratio of 15:1 (elastomer:curing agent) with hexane (Sigma

520 296090) at a ratio of 1:10 (PDMS:hexane) (Koschwanez, Carlson, & Meldrum, 2009;

521 Thangawng, Ruoff, Swartz, & Glucksberg, 2007). A 50 µl filtered (0.5 µm pore size

522 PVDF filter – Millipore) aliquot of bacteria grown to mid-exponential phase and

523   concentrated from 2-5 ml of culture was deposited onto the hydrophobic surface of a

524   PDMS-coated coverslip and incubated for ~20 min to increase surface interactions

525   between bacteria and the coverslip. 7H9 medium (~3 ml) was supplied to the sample

526   so as to immerse the bacterial sample and the AFM cantilever in fluid. The AFM

527   imaging mode, Peak Force QNM, was used to image bacteria with a Nanoscope 5

528   controller (Veeco Metrology) at a scan rate of 0.5 Hz and a maximum Z-range of 12 µm.

529   A ScanAsyst fluid cantilever (Bruker) was used. Height, peak force error, DMT

530   modulus, and log DMT modulus were recorded for all scanned images in the trace and

531   retrace directions. Images were processed using Gwyddion (Department of

532   Nanometrology, Czech Metrology Institute). ImageJ was used for extracting bacterial

533   cell profiles in a tabular form.

534

535   <u>Correlated optical fluorescence and AFM</u>

536   Correlated optical fluorescence and AFM images were acquired as described

537   (Eskandarian et al., 2017). Briefly, optical fluorescence images were acquired with an

538   electron-multiplying charge-coupled device (EMCCD) iXon Ultra 897 camera (Andor)

539   mounted on an IX81 inverted optical microscope (Olympus) equipped with an

540   UPLFLN100XO2PH x100 oil immersion objective (Olympus). Transmitted light

541   illumination was provided by a 12V/100W AHS-LAMP halogen lamp. An U-MGFPHQ

542   fluorescence filter cube for GFP with HQ-Ion-coated filters was used to detect GFP

543   fluorescence. The AFM was mounted on top of the inverted microscope, and images

544   were acquired with a Dimension Icon scan head (Bruker) using ScanAsyst fluid

545   cantilevers (Bruker) with a nominal spring constant of 0.7 N m^{-1} in Peak Force QNM

546   mode at a force setpoint ~1nN and typical scan rates of 0.5 Hz. Indentation on the cell

547   surface was estimated to be ~10 nm in the Z-axis. Optical fluorescence microscopy

548   was used to identify Wag31-GFP puncta expressed in a wild-type background(Dhar et

549   al., 2013) in order to distinguish them from cells of the ΔLDT mutant strains.

550

551   <u>Calculating cell surface rigidity</u>

552   A cell profile was extracted from AFM Height and DMT Modulus image channels as

553   sequentially connected linear segments following the midline of an individual cell. A

554   background correction was conducted to by dividing the DMT modulus values of the cell

555   surface by the mean value of the PDMS surface and rescaled to compare the cell

556   surface rigidity between individual cells from different experiments. The DMT modulus

557   reflects the elastic modulus (stress-strain relationship) for each cross-sectional

558   increment along the cell length.

559

560   <u>Analysis of fluorescent protein distribution</u>

561   Using a segmented line, profiles of cells from new to old pole were created at the frame

562   "pre-division" based on physical cell separation of the phase image. A custom FIJI

563   (Schindelin et al., 2012) script was run to extract fluorescence line profiles of each cell

564   and save them as .csv files. These .csv files were imported to Matlab where a custom

565   script was applied to normalize the fluorescence line profile to fractional cell length and

566   to interpolate the fluorescence values to allow for averaging.

567

568   <u>Analysis of cell wall distribution</u>

569　Cells were stained with Alexa488 NHS ester as described previously (Aldridge et al.,

570　2012) and followed via time-lapse microscopy in the CellASIC device. Briefly, 1mL of

571　log phase cells was pelleted at 8,000 rpm for 1 minute and washed with 1mL PBST.

572　The pellet was resuspended in 100uL of PBST and 10uL Alexa Fluor 488 carboxylic

573　acid succinimidyl ester was added for a final concentration of 0.05mg/mL. This was

574　incubated for 3 minutes at room temperature. Stained cells were pelleted for 1 minute at

575　13,000 rpm and washed with 500μL PBST. They were spun again and resuspended in

576　7H9 for outgrowth observation over time in the CellASIC device.

577

578　Analysis of FDAAs

579　Images were analyzed using a combination of Oufti (Paintdakhi et al., 2016) for cell

580　selection followed by custom coded Matlab scripts to plot FDAA fluorescence over

581　normalized cell length, calculate cell length and bin cells by existence of an FDAA

582　labeled septum.

583

584　Generation of transposon libraries

585　*M. smegmatis* cells were transduced at (OD$_{600}$ 1.1-1.7) with φMycoMarT7 phage

586　(temperature sensitive) that has a Kanamycin marked Mariner transposon as previously

587　described (Long et al., 2015). Briefly, mutagenized cells were plated at 37°C on LB

588　plates supplemented with Kanamycin to select for phage transduced cells. Roughly

589　100,000 colonies per library were scraped, and genomic DNA was extracted.

590　Sequencing libraries were generated specifically containing transposon disrupted DNA.

591　Libraries were sequenced on the Illumina platform. Data were analyzed using the

592   TRANSIT pipeline (DeJesus et al., 2015).

593   Peptidoglycan isolation and analysis

594   600mLs of wildtype and ΔLDT cells were grown to log phase and collected via

595   centrifugation at 5000 x g for 10 minutes at 4°C. The resulting pellet was resuspsended

596   in PBS and cells were lysed using a cell disruptor at 35,000psi twice. Lysed cells were

597   boiled in 10% SDS (sodium dodecyl sulfate) for 30 minutes and peptidoglycan was

598   collected via centrifugation at 17,000 x g. Pellets were washed with 0.01% DDM(n-

599   Dodecyl β-D-maltoside) to remove SDS and resuspended in 1XPBS + 0.01% DDM. PG

600   was digested with alpha amylase (Sigma A-6380) and alpha chymotrypsin (Amersco

601   0164) overnight. The samples were again boiled in 10% SDS and washed in 0.01%

602   DDM. The resulting pellet was resuspended in 400μL 25mM sodium phosphate pH6,

603   0.5mM MgCl2, 0.01% DDM. 20μL of lysozyme (10mg/mL) and 20μL 5U/μL

604   mutanolysoin (Sigma M9901) were added and incubated overnight at 37°C. Samples

605   were heated at 100°C and centrifuged at 100,000 x g. 128μL of ammonium hydroxide

606   was added and incubated for 5 hours at 37°C. This reaction was neutralized with 122μL

607   of glacial acetic acid. Samples were lyophilized, resuspended in 300μL 0.1% formic acid

608   and subjected to analysis by LC-MS/MS. Peptide fragments were separated with an

609   Agilent Technologies 1200 series HPLC on a Nucleosil C18 column (5μm 100A 4.6 x

610   250mm) at 0.5mL/min flow rate with the following method: Buffer A= 0.1% Formic Acid;

611   Buffer B=0.1% Formic Acid in acetonitrile; 0% B from 0-10 minutes, 0-20% B from 10-

612   100 minutes, 20% B from 100-120 minutes, 20-80% B from 120-130 minutes, 80% B

613   from 130-140 minutes, 80%-0% B from 140- 150minutes, 0% B from 150-170 minutes.

614 MS/MS was conducted in positive ion mode using electrospray ionization on an Agilent

615 Q-TOF (6520).

616

617 <u>Expression and purification of MSMEG_2433 (DacB2)</u>

618 MSMEG_2433 was expressed and purified using a modified method for purification of

619 low molecular weight PBPs that was previously published (Qiao et al., 2014). An N-

620 terminally truncated MSMEG_2433$_{(29\text{-}296)}$ was cloned into the pET28b vector for isopropyl

621 β-D-1-thiogalactopyranoside (IPTG) inducible expression in *E. coli* BL21 (DE3). 10mLs

622 of overnight culture grown in LB with Kanamycin (50μg/mL) were diluted 1:100 into 1 L of

623 LB with Kanamycin (50μg/mL) and grown at 37°C until an OD$_{600}$ of 0.5. The culture was

624 cooled to room temperature, induced with 0.5mM IPTG, and shaken at 16°C overnight.

625 Cells were pelleted via centrifugation at 4,000rpm for 20 min at 4°C. The pellet was

626 suspended in 20mL binding buffer (20mM Tris pH 8, 10mM MgCl$_2$, 160mM NaCl, 20mM

627 imidazole) with 1mM phenylmethylsulfonylfluoride (PMSF) and 500µg/mL DNase. Cells

628 were lysed via three passage through a cell disrupter at $\geq$ 10,000 psi. Lysate was pelleted

629 by ultracentrifugation (90,000 × g, 30 min, 4°C). To the supernatant, 1.0mL washed Ni-

630 NTA resin (Qiagen) was added and the mixture rocked at 4°C for 40 min. After loading

631 onto a gravity column, the resin was washed twice with 10mL wash buffer (20mM Tris pH

632 8, 500mM NaCl, 20mM imidazole, 0.1% Triton X-100). The protein was eluted in 10mL of

633 elution buffer (20 mM Tris pH8, 150mM NaCl, 300mM imidazole, 0.1% reduced Triton X-

634 100) and was concentrated to 1 mL with a 10kD MWCO Amicon Ultra Centrifuge Filter.

635 The final protein concentration was measured by reading absorbance at 280 nm and

636 using the estimated extinction coefficient (29459 M^{-1}cm^{-1}) calculate concentration. The

637   protein was diluted to 200μM in elution buffer with 10% glycerol, aliquoted, and stored at

638   -80°C.

639   Proper folding of purified MSMEG_2433$_{(29-296)}$ was tested via Bocillin-FL binding. Briefly,

640   20μM of purified protein was added to penicillin G (100, 1000 U/mL in 20mM K_2HPO_4,

641   140mM NaCl, pH7.5) in a 9μL reaction. The reaction was incubated at 37°C for 1hour.

642   10μM Bocillin-FL was added and incubated at 37°C for 30 minutes. SDS loading dye

643   was added the quench the reaction and samples were loaded onto a 4-20% gel.

644   MSMEG_2433$_{(29-296)}$ bound by Bocillin-FL was imaged using a Typhoon 9400 Variable

645   Mode Imager (GE Healthcare) (Alexa Excitation-488nm Emission-526nm).

646

647   Lipid II extraction.

648   *B. subtilis* Lipid II was extracted as previously published (Qiao et al., 2017).

649

650   SgtB purification.

651   *S. aureus* SgtB was purified as previously published (Rebets et al., 2014).

652

653   Purification of *B. subtilis* PBP1.

654   Purification of *B. subtilis* PBP1 was carried out as previously described (Lebar et al.,

655   2014).

656

657   *In vitro* Lipid II polymerization and crosslinking.

658   20 μM purified BS Lipid II was incubated in reaction buffer (50 mM HEPES pH 7.5, 10

659   mM $CaCl_2$) with either 5 μM PBP1 or 0.33 μM SgtB for 1 hour at room temperature. The

33

660   enzymes were heat denatured at 95°C for 5 minutes. Purified MSMEG_2433$_{(29-296)}$ was

661   added (20 uM, final) and the reaction was incubated at room temperature for 1 hour.

662   Mutanolysin (1 μL of a 4000 U/mL stock) was added and incubated for 1.5 hours at 37

663   °C (twice). The resulting muropeptides were reduced with 30 μL of NaBH$_4$ (10 mg/mL)

664   for 20 minutes at room temperature with tube flicking every 5 minutes to mix. The pH

665   was adjusted to ~4 using with 20% H$_3$PO$_4$ and the resulting product was lyophilized to

666   dryness. The residue was resuspended in 18μL of water and analyzed via LC-MS as

667   previously reported (Welsh et al., 2017).

668

669
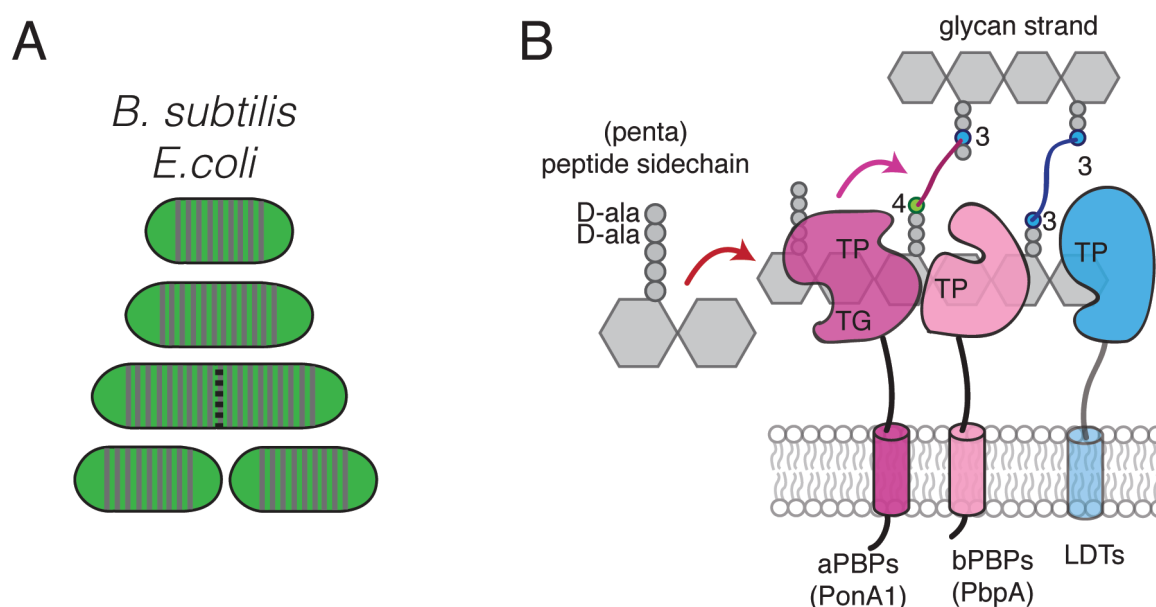
670
671 **Figure 1- figure supplement 1: Peptidoglycan synthesis and FDAA screen**
672 **overview. (A)** *Escherichia coli* and *Bacillus subtilis* lateral cell wall growth. Unlike
673 mycobacteria, *E. coli* and *B. subtilis* insert new cell wall along the lateral cell body, mixing
674 old and new peptidoglycan. Green portion represents old cell wall; grey portion represents
675 new material. **(B)** Cartoon of penicillin binding proteins (PBPs), L,D-transpeptidases
676 (LDTs), and both 4-3 and 3-3 crosslinking. PBPs utilize a pentapeptide substrate found
677 on new peptidoglycan, ending in D-alanine-D-alanine. LDTs utilize a tetrapeptide
678 substrate found on processed peptidoglycan. TP, transpeptidase; TG, transglycosylase
679
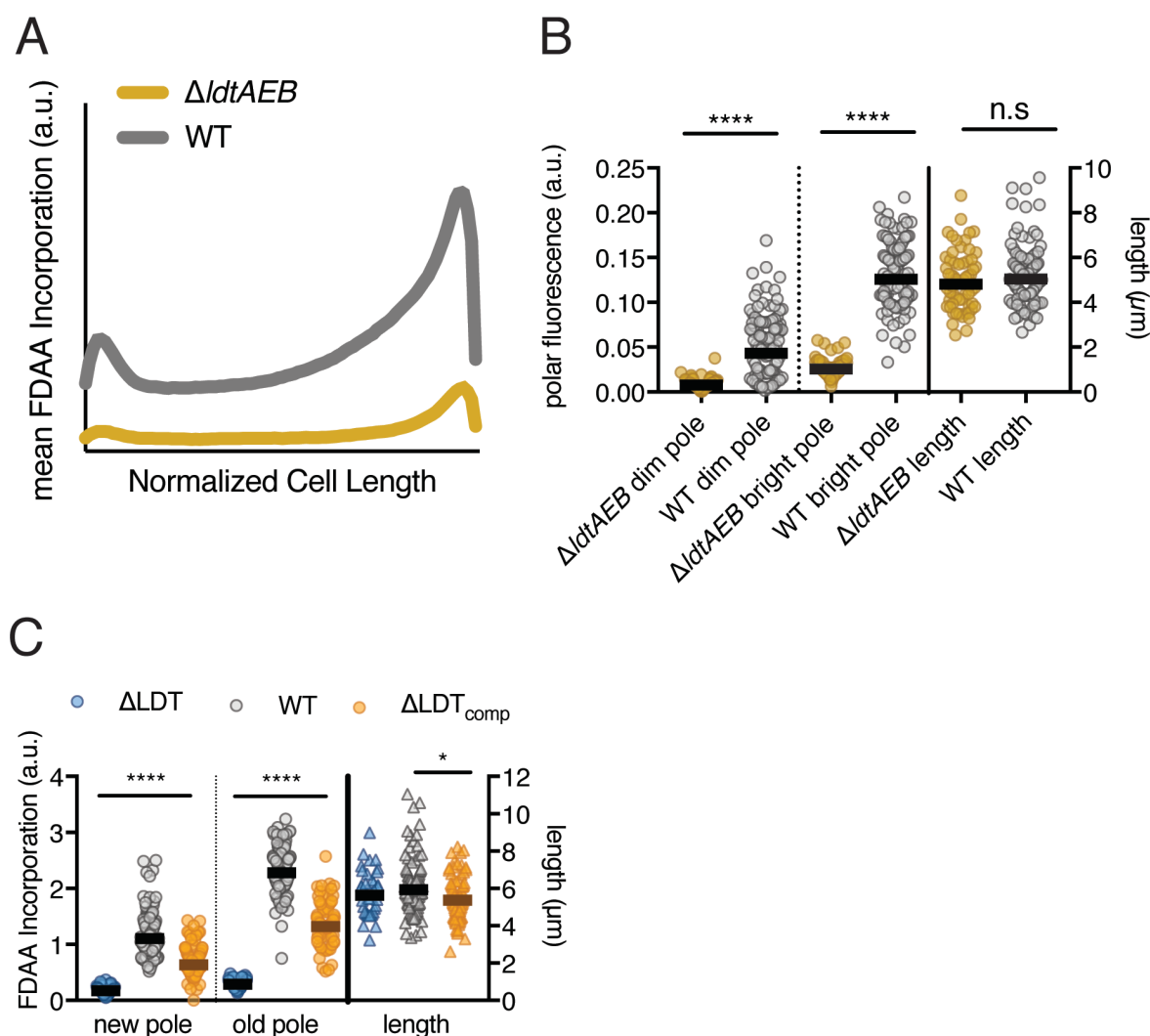
680
681 **Figure 1- figure supplement 2: Fluorescent D-amino acid screen validation. (A)**
682 Mean line profiles (from new to old pole) of FDAA incorporation in log-phase WT (N=97),
683 *ΔldtABE* (N=64). **(B)** Quantification of FDAA incorporation at cell poles and quantification
684 of cell length. Mann-Whitney U P-Value shown (**** P-Value < 0.0001). **(C)** Quantification
685 of FDAA incorporation at poles and cell lengths of WT, ΔLDT and ΔLDT$_{comp}$ cells shown
686 in Fig. 1E and whose mean incorporation is shown in Fig. 1F.
687
688

689

A

WT

B

| PEAK	Tripeptides observed	Description*
1	461.2	
	Tetrapeptides observed	
2	532.3	Tetra (2 NH2)
3	534.2	Tetra (OH)
4	533.2	Tetra (NH2)
	pentapeptides observed	
5	604.3	Penta (OH)
6	602.3	Penta(2 NH2)
	4-3 observed	
7	974.5	4--3 (2 NH2)
8	1045.4	4--4 (4 NH2)
9	1046.5	4--4 (3 NH2)
10	1049.4	4--4
11	975.4	4--3 (NH2)
12	974.3	4--3 (2 NH2)
13	1047.5	4--4 (2 NH2)
	3-3 observed	
14	974.4	4--3 (4 NH2)
15	904.4	3--3 (3 NH2)
16	975.5	4--3 (3 NH2)
	Tripeptide(anhydrous)	
17	865.4	
	4--4--4	
18	1559.7	
19	1560.0	

C

3-3 crosslink (tripeptide-tripeptide)
m/z: 904.44 (100.0%), 905.44 (38.9%),
906.44 (7.4%), 905.43 (4.1%), 906.44 (3.3%),
906.44 (1.6%), 907.44 (1.3%)

D

Figure 1- figure supplement 3: 3-3 crosslinks are not detectable in ΔLDT cells. (A) Total ion chromatograms of WT, ΔLDT and ΔLDT$_{comp}$ peptidoglycan. (B) Table of

690
691

37

692   muropeptide masses (Da) observed in (S3A). The molecular weight difference by one of
693   the identified peptides is due to differential amidation. The descriptions include the
694   peptide lengths in the crosslink (4= tetra-, 3= tri- peptide) and the following parenthesis
695   specifies the number of amidation in the species according to mass. **(C)** Structure of a
696   representative 3-3 crosslink with a m/z=904.4. **(D)** Extracted ion chromatograms from
697   WT, ΔLDT and ΔLDT$_{comp}$ for a representative 3-3 crosslink with a m/z=904.4.
698

699

700
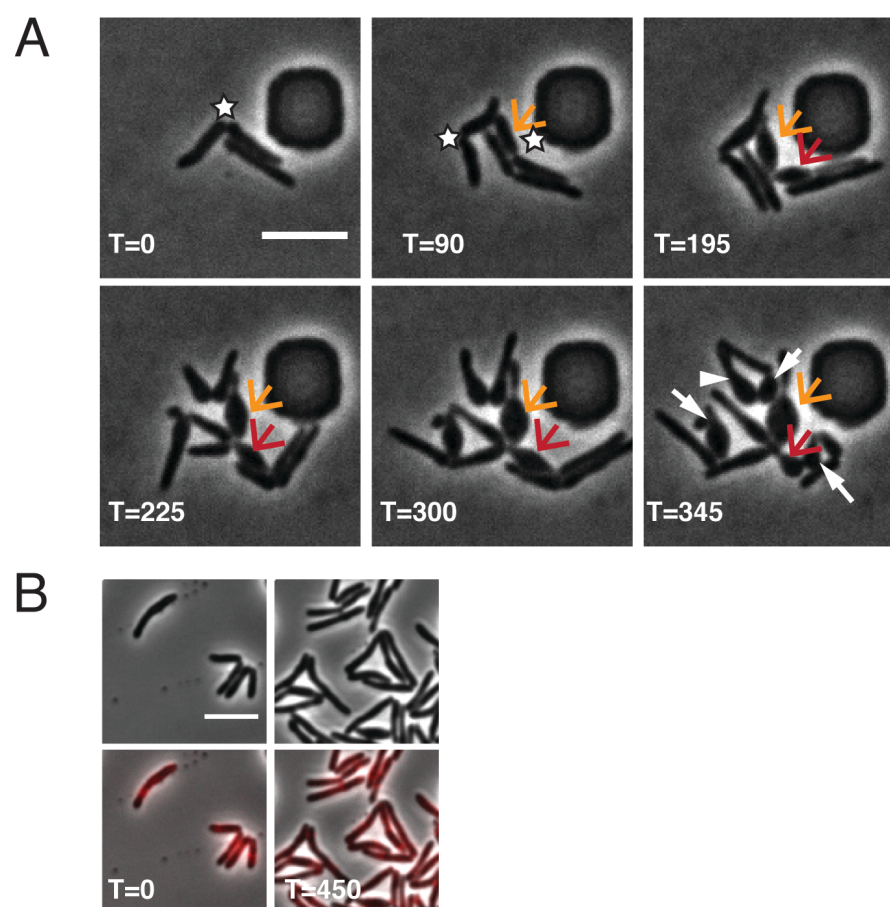
Figure 2- figure supplement 1: ΔLDT cell morphological characteristics. (A) Time-
lapse microscopy montage of ΔLDT cells. The white stars mark new poles. The orange
arrow points to the first new pole daughter cell of this series. The red arrow indicates the
second resulting new pole daughter cell. In the last frame, white arrows point to all new
pole daughter cells (besides the orange arrow and red arrow). **(B)** Time-lapse microscopy
montage of ΔLDT$_{comp}$ cells expressing LdtE-mRFP.
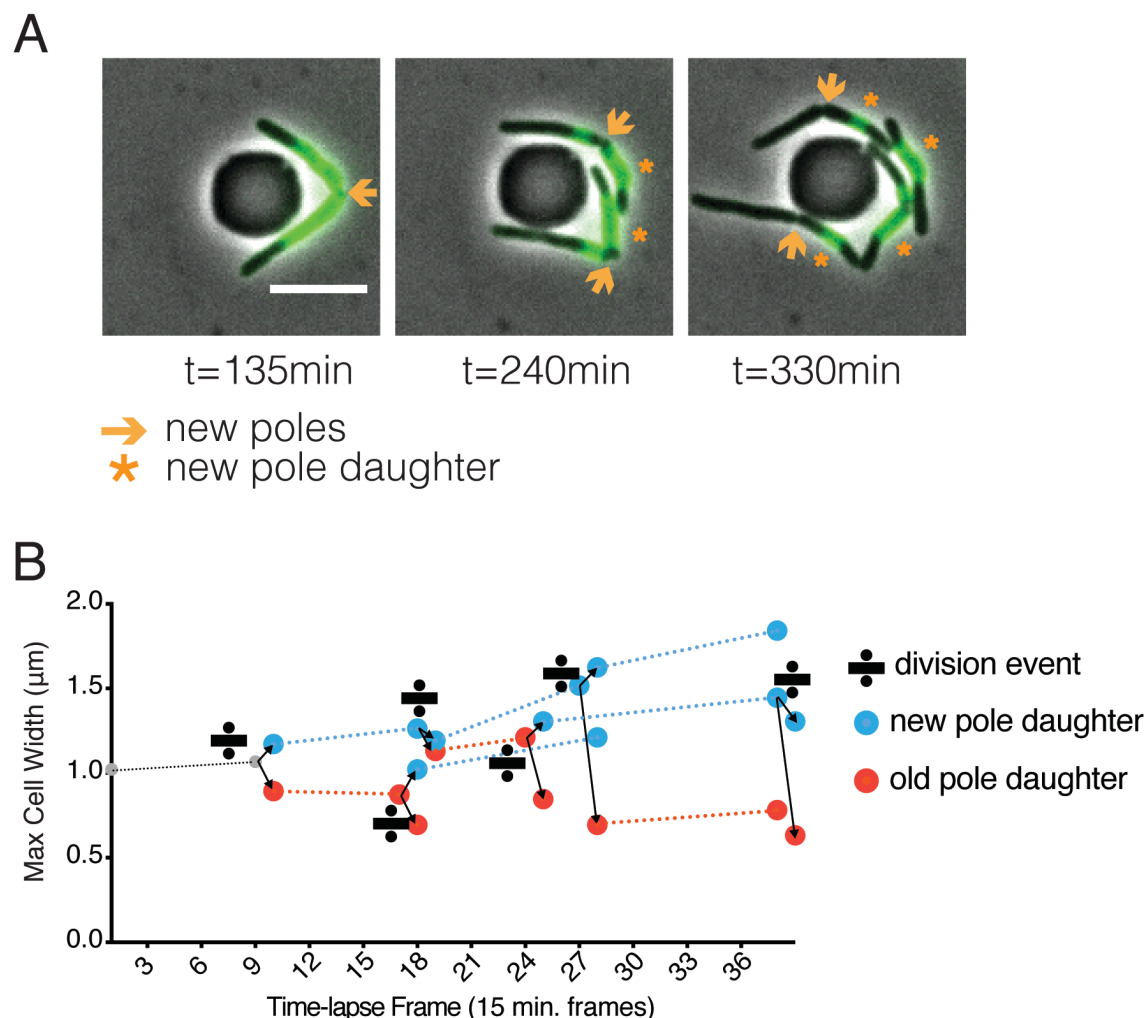All scale bars=5μm

708

Figure 2- figure supplement 2: Inheritance of old cell wall and occurrence of blebs in new pole daughter cells. (A) WT Msm stained with Alexa Fluor™ 488 NHS ester, washed and visualized over time. New material is unstained, old material is stained green. Orange arrows indicate a new pole. Orange stars mark new pole daughter cells. All scale bars=5μm **(B)** Maximum cell width of ΔLDT cell lineages over time. Width of new pole daughters = blue circle; width of old pole daughters = orange circle. Division signs denote a division event. At each division, there are two arrows from the dividing cell leading to the resulting new and old pole daughter cell widths (blue and orange respectively).

720
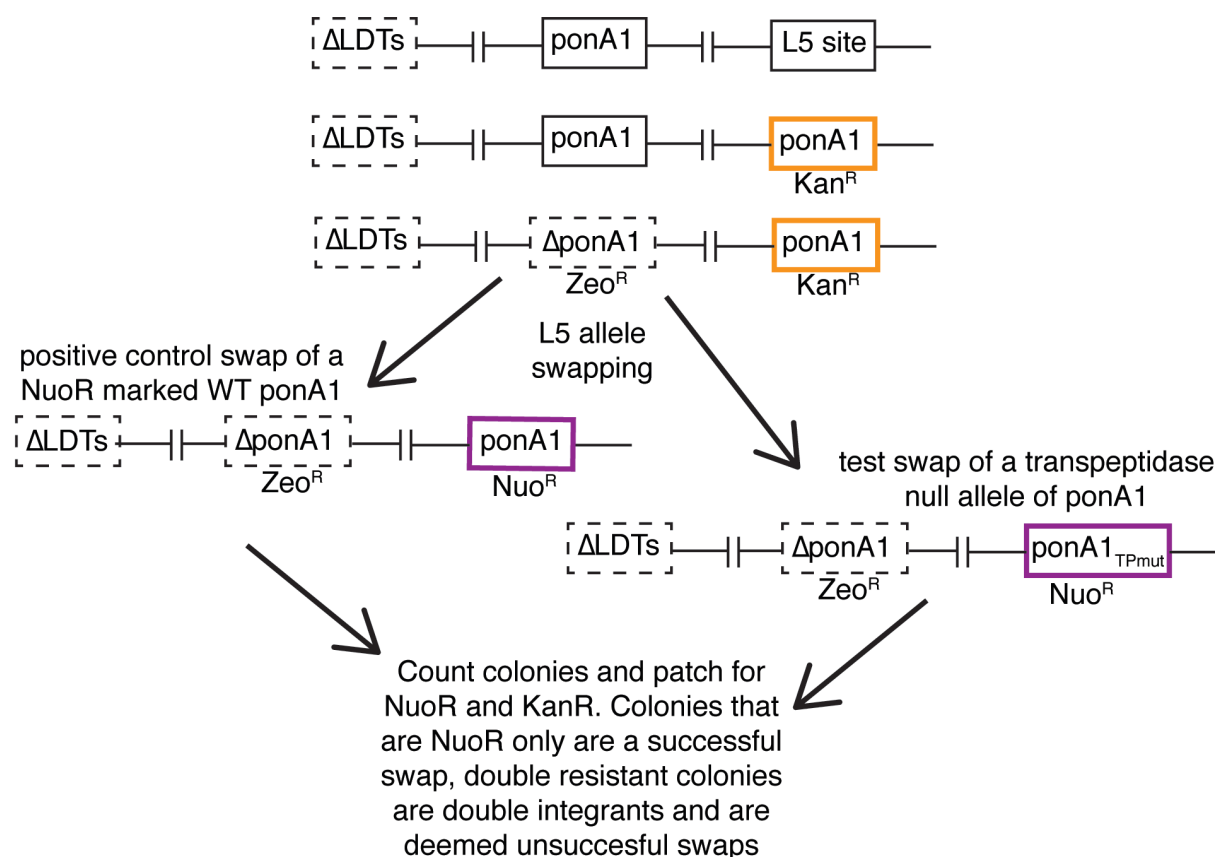
Figure 3- figure supplement 1: L5 allele swapping to test essentiality of PonA1's ability to form 4-3 crosslinks (transpeptidation). (A) Schematic of L5 allele swapping experiment. Adapted from (Kieser, Boutte, et al., 2015b).

724
725

726

727

728 **Figure 4- figure supplement 1: MSMEG_2433 (DacB2) functions as a D,D-**
729 **carboxypeptidase and D,D-endopeptidase *in vitro*. (A)** Coomassie-stained gel of
730 purified His$_6$-DacB2. **(B)** Bocillin-FL and Penicillin G binding assay of purified DacB2.
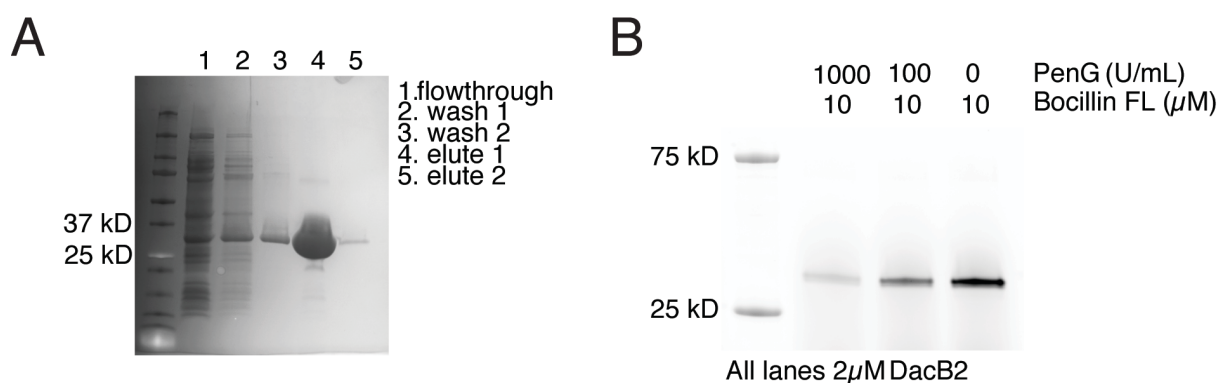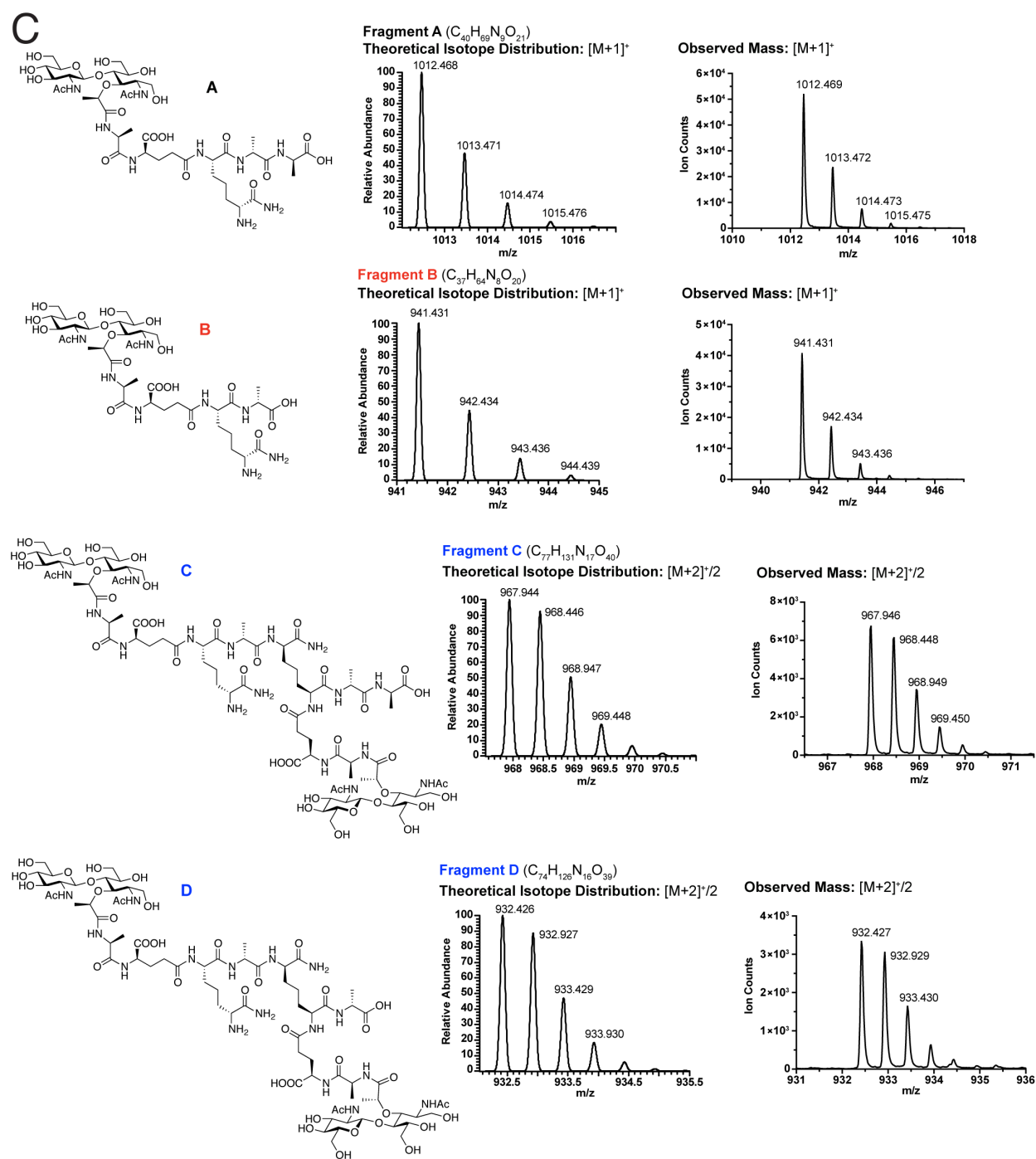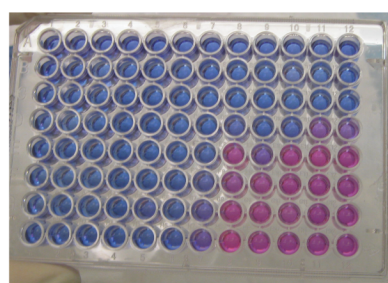
731

732

Figure 4- figure supplement 1 (continued): MSMEG_2433 (DacB2) functions as a D,D-carboxypeptidase and D,D-endopeptidase *in vitro*. (C) Mass spectra of the reaction products of DacB2 digestion reactions.

736

737

738

A

	1	2	3	4	5	6	7	8	9	10	11	12
A	10.00	10.00	10.00	10.00	10.00	10.00	10.00	10.00	10.00	10.00	10.00	
	10.00	5.00	2.50	1.25	0.63	0.31	0.16	0.08	0.04	0.02	0.01	
B	5.00	5.00	5.00	5.00	5.00	5.00	5.00	5.00	5.00	5.00	5.00	
	10.00	5.00	2.50	1.25	0.63	0.31	0.16	0.08	0.04	0.02	0.01	
C	2.50	2.50	2.50	2.50	2.50	2.50	2.50	2.50	2.50	2.50	2.50	
	10.00	5.00	2.50	1.25	0.63	0.31	0.16	0.08	0.04	0.02	0.01	
D	1.25	1.25	1.25	1.25	1.25	1.25	1.25	1.25	1.25	1.25	1.25	
	10.00	5.00	2.50	1.25	0.63	0.31	0.16	0.08	0.04	0.02	0.01	
E	0.63	0.63	0.63	0.63	0.63	0.63	0.63	0.63	0.63	0.63	0.63	
	10.00	5.00	2.50	1.25	0.63	0.31	0.16	0.08	0.04	0.02	0.01	
F	0.31	0.31	0.31	0.31	0.31	0.31	**0.31**	0.31	0.31	0.31	0.31	
	10.00	5.00	2.50	1.25	0.63	0.31	**0.16**	0.08	0.04	0.02	0.01	
G	0.16	0.16	0.16	0.16	0.16	0.16	0.16	0.16	0.16	0.16	0.16	
	10.00	5.00	2.50	1.25	0.63	0.31	0.16	0.08	0.04	0.02	0.01	
H	0.08	0.08	0.08	0.08	0.08	0.08	0.08	0.08	0.08	0.08	0.08	
	10.00	5.00	2.50	1.25	0.63	0.31	0.16	0.08	0.04	0.02	0.01	

B

	1	2	3	4	5	6	7	8	9	10	11	12	
A	40.00	20.00	10.00	5.00	2.50	1.25	**0.63**	0.31	0.16	0.08	0.04	0.02	amoxicillin
B	40.00	20.00	10.00	5.00	2.50	1.25	**0.63**	0.31	0.16	0.08	0.04	0.02	
C	40.00	20.00	10.00	5.00	2.50	**1.25**	0.63	0.31	0.16	0.08	0.04	0.02	meropenem
D	40.00	20.00	10.00	5.00	2.50	**1.25**	0.63	0.31	0.16	0.08	0.04	0.02	

739

740 **Figure 5- figure supplement 1: Minimum inhibitory concentration (MIC) of**
741 **amoxicillin or meropenem alone or in combination against *Mycobacterium***

44

742   *tuberculosis*. **(A)** Resazurin MIC plate and dilution matrix of amoxicillin and meropenem
743   in combination in a checkerboard MIC plate. The table below shows the concentration of
744   each drug per well in μg/mL. The concentration of meropenem is in black text and the
745   concentration of amoxicillin is in red text in each well. **(B)** Dilution matrix of amoxicillin or
746   meropenem (alone). The concentrations of drugs are shown in the table. Pink indicates
747   metabolically active cells, blue indicates not metabolically active. In both single drug and
748   checkerboard MIC plates, 5μg/mL clavulanate was used.
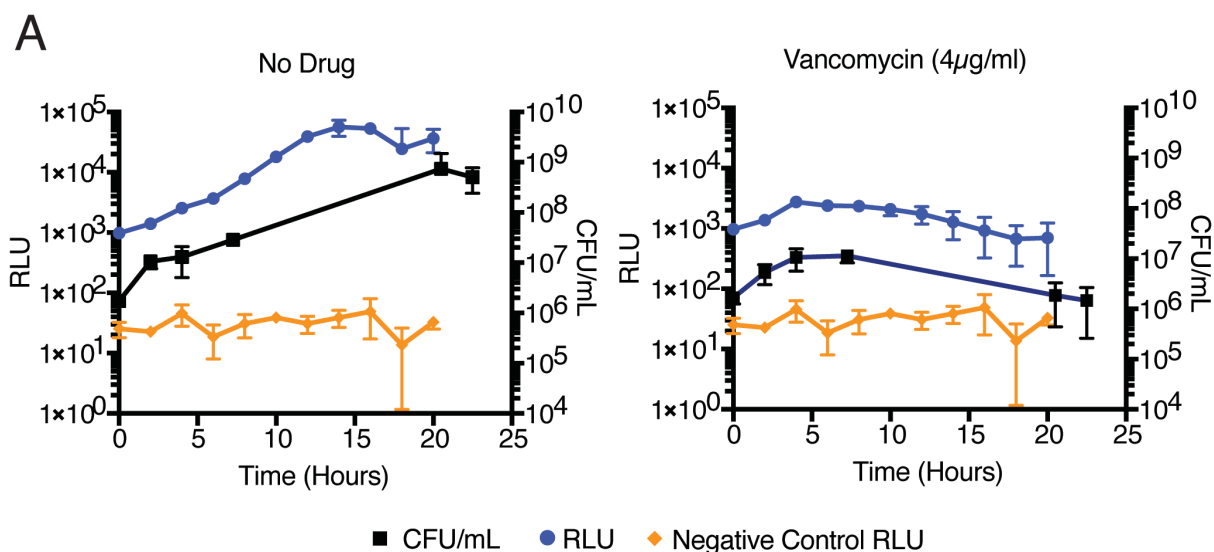749

750

751

Figure 5- figure supplement 2: Light production (RLU) correlated to colony forming units (CFU) in mycobacterial cells expressing *luxABCDE* in drug treatment. (A) *Mycobacterium smegmatis* colony forming units (CFU) and luminescence (RLU) during drug treatment.

756

757 **Video captions**

758

759 **Figure 2-video1- Time-lapse of ΔLDT cells in iso-osmolar media.**
760 This video corresponds to Figure 2A (top). This is a time-lapse microscopy video of
761 ΔLDT Msm cells growing in 7H9 (iso-osmolar) media. Frames are 15 minutes apart, and
762 the video is 5 frames/second.

763

764 **Figure 2-video2- Time-lapse of ΔLDT cells in high-osmolar media.**
765 This video corresponds to Figure 2A (bottom). This is a time-lapse microscopy video of
766 ΔLDT Msm cells growing in 7H9 +150mM sorbitol (high-osmolar) media. Frames are 15
767 minutes apart, and the video is 5 frames/second.

768
769

770 **Figure 4-video1- Time-lapse of ponA1-RFP.**
771 This video corresponds to Figure 4A,B. This is a time-lapse microscopy video of Msm
772 cells expressing ponA1-RFP growing in 7H9 media. Frames are 15 minutes apart, and
773 the video is 5 frames/second.

774

775 **Figure 4-video2- Time-lapse of ldtE-mRFP.**
776 This video corresponds to Figure 4A,B. This is a time-lapse microscopy video of Msm
777 cells expressing ldtE-mRFP growing in 7H9 media. Frames are 15 minutes apart, and
778 the video is 5 frames/second.

779

780 **Figure 4-video3- Time-lapse of dacB2-mRFP.**
781 This video corresponds to Figure 4A,B. This is a time-lapse microscopy video of Msm
782 cells expressing dacB2-mRFP growing in 7H9 media. Frames are 15 minutes apart, and
783 the video is 5 frames/second.

784
785
786

787
788 **Supplementary table 1: List of Primers**
789

Primer description	Primer Sequence	5' or 3' features	Primer #
MSMEG_3528 (ldtA) upstream flanking region FOR	CGTTGTAAAACGACGGCCAGTGATGGCGGGCGTGATCTGGAATCTCT	pUC57 overlap	208
MSMEG_3528 (ldtA) upstream flanking region REV	ACCCAACTTAATCGCCTTGCAGCTCTTCCAGTGTAGGTTGTCGAAACG	Zeo cassette overlap	209
MSMEG_3528 (ldtA) downstream flanking region FOR	TAATCATGGTCATAGCTGTTTTCATCGTGCAGGCGTGACGTGCAG	Zeo cassette overlap	210
MSMEG_3528 (ldtA) downstream flanking region REV	CAGTCGACGGGCCCGGGATCCGCGGTGGTGCCCTTGGTGATGGTC	pUC57 overlap	211
MSMEG_0233 (ldtE) upstream flanking region FOR	CGTTGTAAAACGACGGCCAGTGGCTGTCCGCCCAGCCCCGGGCC	pUC57 overlap	220
MSMEG_0233 (ldtE) upstream flanking region REV	CCAACTTAATCGCCTTGCAGCGTGGTACCTCCAGAGCACAACTG	Zeo cassette overlap	221
MSMEG_0233 (ldtE) downstream flanking region FOR	GTAATCATGGTCATAGCTGTTTCCGGACGTCATACGAAGAACCCCC	Zeo cassette overlap	222
MSMEG_0233 (ldtE) downstream flanking region REV	GCAGTCGACGGGCCCGGGATCTGGACCGACGCCGACCGCACCG	pUC57 overlap	223
MSMEG_4745 (ldtB) upstream flanking region FOR	GGTCGAGATGCTCCTGGAAGAGGCCG		444

MSMEG_4745 (ldtB) upstream flanking region REV	GAGCTCCAATTCGCCCTACG TCGTTACCTGCCCCATCACG	hyg cassette overlap	445
MSMEG_4745 (ldtB) downstream flanking region FOR	GTACCTCGAGTCTAGAAGTA GCGCTATCGCACCGCGCGGT CCAG	hyg cassette overlap	446
MSMEG_4745 (ldtB) downstream flanking region REV	CGACCCGGCCCGTCACAAGG ACACCGAAC		447
MSMEG_0929 (ldtC) upstream flanking region FOR	CGTTGTAAAACGACGGCCAG TGAACTGGCGACGGCGCTGG GCGTGG	pUC57 overlap	216
MSMEG_0929 (ldtC) upstream flanking region REV	TGGAGCTCCAATTCGCCCTA GTGGATCTAGGGTACCGACA GCACGC	hyg cassette overlap	448
MSMEG_0929 (ldtC) downstream flanking region FOR	GGTACCTCGAGTCTAGAAGT AGTCCGGCGGCTAGGTCCG GCGGTTGAAG	hyg cassette overlap	449
MSMEG_0929 (ldtC) downstream flanking region REV	CAGTCGACGGGCCCGGGAT CCCAAGGGACTCGCGCCGGT CTCC	pUC57 overlap	219
MSMEG_0929 (ldtC) upstream flanking region FOR	GGCTCGTTCTTCACCAACC		507
MSMEG_0929 (ldtC) downstream flanking region REV	CTGCCCAAGCTCATCGAC		508
MSMEG_0674 (ldtG) upstream flanking region FOR	GTTGTAAAACGACGGCCAGT GCGGCGTCGACCTCCCGGC CGGGTC	pUC57 overlap	228

MSMEG_0674 (ldtG) upstream flanking region REV	GTGGAGCTCCAATTCGCCCT AGCGCATTGGCTTCCGATTT CCCTCG	hyg cassette overlap	454
MSMEG_0674 (ldtG) downstream flanking region FOR	CGGTACCTCGAGTCTAGAAG TACGCCGACGTGTATGCCCA CCCCCGCG	hyg cassette overlap	455
MSMEG_0674 (ldtG) downstream flanking region REV	GCAGTCGACGGGCCCGGGA TCGCCTGCGCCCGCGGGAG CGCCTGCC	pUC57 overlap	231
MSMEG_0674 (ldtG) upstream flanking region FOR	GCATCTGAGTTTCGGCAAG		513
MSMEG_0674 (ldtG) downstream flanking region REV	CAACTACCCCGCAGTTGAAT		514
MSMEG_1322 (ldtF) upstream flanking region FOR	GTTGTAAAACGACGGCCAGT GCGAGGTAAGGGTCTCGACG GTTTCT	pUC57 overlap	224
MSMEG_1322 (ldtF) upstream flanking region REV	GTGGAGCTCCAATTCGCCCT ATCCAATGTGCTTCGGCGAA AGCCAGTTTG	hyg cassette overlap	452
MSMEG_1322 (ldtF) downstream flanking region FOR	GTACCTCGAGTCTAGAAGTA GTTCCCCCCGGCCCACATAT GTCTGGACG	hyg cassette overlap	453
MSMEG_1322 (ldtF) downstream flanking region REV	GCAGTCGACGGGCCCGGGA TCCACGACAACGCCAGCGCG AT	pUC57 overlap	227
MSMEG_1322 (ldtF) upstream flanking region FOR	GGTCGACGACGAACTGGT		511
MSMEG_1322 (ldtF) downstream	AACGGCACGTACATCAGGAC		512

flanking region REV			
MSMEG_0233 (ldtE) FOR with TetO overlap (vector)	CATGCTTAATTAAGAAGGAGA TATACAATGCCGAAATCGGC AAAACGCAG		323A
MSMEG_0233 (ldtE) REV (no stop codon) with ser-ser-gly linker	GATGACGTCCTCGGAGGAGG CCGAGCCGCCGAACATCTGC CAGTCGGATG		351
mRFP FOR with ser-ser-gly linker	CATCCGACTGGCAGATGTTC GGCGGCTCGGCCTCCTCCGA GGACGTCATC		352
mRFP REV with vector overlap	GTCCCCAATTAATTAGCTAAG TGATGGTGATGGTGATGACA GGCG		353
MSMEG_2433 (dacB2) FOR (first 27 amino acids truncated)	GGCCTGGTGCCGCGCGGCA GCCATCGCGCGGACGCCGA CATCCAG	with 5' overlaps to pet28b cut with NdeI	662
MSMEG_2433 (dacB2) REV	GCTGTCCACCAGTCATGCTA GCCATCAGAGCGCCCCGATG CTCG	with 3' overlaps to pet28b cut with NdeI	663

790
791

Supplementary Table 2: List of Strains

Strain	Description	Primers
KB134	mc2155Δ*ldtA*::loxP	208/209; 210/211
KB156	mc2155Δ*ldtA*::loxP + Δ*ldtE*:: zeoR	220/221; 222/223
KB200	mc2155Δ*ldtA*::loxP Δ*ldtE*:: zeoR + Δ*ldtB*:: hygR	444/445; 446/447
KB209	mc2155Δ*ldtA*::loxP Δ*ldtE*::loxP Δ*ldtB*::loxP + Δ*ldtC*:: hygR	216/448; 449/219 (create original hyg KO) but used 507/508; (amplify KO from strain within the flanks)
KB222	mc2155Δ*ldtA*::loxP Δ*ldtE*::loxP Δ*ldtB*::loxP Δ*ldtC*:: hygR Δ*ldtG*:: zeoR	228/454; 455/231 (create original hyg KO) but used 513/514; (amplify KO from strain within the flanks)
KB303 (ΔLDT)	mc2155Δ*ldtA*::loxP Δ*ldtE*::loxP Δ*ldtB*::loxP Δ*ldtC*:: loxP Δ*ldtG*:: loxP Δ*ldtF*:: hygR	224/452; 453/227 (create hyg KO) but used 511/512 (amplify KO from strain or gibson)
KB302	pTetO-ldtE(MSMEG_0233)-linker-mRFP in CT94 XH (XL1-Blue)	323A/351; 352/353
KB316 (ΔLDTcomp)	[mc2155ΔldtA::loxP ΔldtE::loxP ΔldtB::loxP ΔldtC:: loxP ΔldtG:: loxP ΔldtF:: hygR] + KB302	
KB428	*E.coli* BL21 + pet28b (dacB2)	662/663

796 **Supplemental Table 3: FDAA FACs screen data used for Figure 1D**
797
798 **Supplemental Table 4: ΔLDT Tnseq data used for Figure 3A**
799 Below are the column names with a brief description-
800 Orf   - ID of gene
801 Name - name of gene
802 Desc - annotation of gene
803 Sites - number of TA sites in gene
804 Mean Ctrl - mean insertion count averaged over TA sites and replicates for wildtype
805 strain (mc^{2}155)
806 Mean Exp - mean insertion count averaged over TA sites and replicates for knockout
807 strain (ΔLDT)
808 log2FC - log-fold-change, log2(meanExp/meanCtl)
809 Sum Ctrl - sum of insertion counts over TA sites and replicates for wildtype strain
810 (mc^{2}155)
811 Sum Exp   - sum of insertion counts over TA sites and replicates for knockout strain
812 (ΔLDT)
813 Delta Sum - difference of sums (sumExp-sumCtl)
814 p-value - probability of null hypothesis (i.e. no significant difference between strains)
815 estimated from resampling distribution
816 Adj. p-value - p-values after applying Benjamini-Hochberg correction for multiple tests
817
818
819
820
821
822

References:

Aldridge, B. B., Fernandez-Suarez, M., Heller, D., Ambravaneswaran, V., Irimia, D., Toner, M., & Fortune, S. M. (2012). Asymmetry and aging of mycobacterial cells lead to variable growth and antibiotic susceptibility. *Science*, *335*(6064), 100–104. http://doi.org/10.1126/science.1216166

Andreu, N., Fletcher, T., Krishnan, N., Wiles, S., & Robertson, B. D. (2012). Rapid measurement of antituberculosis drug activity in vitro and in macrophages using bioluminescence. *The Journal of Antimicrobial Chemotherapy*, *67*(2), 404–414. http://doi.org/10.1093/jac/dkr472

Andreu, N., Zelmer, A., Fletcher, T., Elkington, P. T., Ward, T. H., Ripoll, J., et al. (2010). Optimisation of bioluminescent reporters for use with mycobacteria. *PLoS ONE*, *5*(5), e10777. http://doi.org/10.1371/journal.pone.0010777

Bansal, A., Kar, D., Murugan, R. A., Mallick, S., Dutta, M., Pandey, S. D., et al. (2015). A putative low-molecular-mass penicillin-binding protein (PBP) of Mycobacterium smegmatis exhibits prominent physiological characteristics of DD-carboxypeptidase and beta-lactamase. *Microbiology (Reading, England)*, *161*(Pt 5), 1081–1091. http://doi.org/10.1099/mic.0.000074

Botella, H., Yang, G., Ouerfelli, O., Ehrt, S., Nathan, C. F., & Vaubourgeix, J. (2017). Distinct Spatiotemporal Dynamics of Peptidoglycan Synthesis between Mycobacterium smegmatis and Mycobacterium tuberculosis. *mBio*, *8*(5), e01183–17. http://doi.org/10.1128/mBio.01183-17

Boutte, C. C., Baer, C. E., Papavinasasundaram, K., Liu, W., Chase, M. R., Meniche, X., et al. (2016). A cytoplasmic peptidoglycan amidase homologue controls mycobacterial cell wall synthesis. *eLife*, *5*, a021113. http://doi.org/10.7554/eLife.14590

Böth, D., Schneider, G., & Schnell, R. (2011). Peptidoglycan remodeling in Mycobacterium tuberculosis: comparison of structures and catalytic activities of RipA and RipB. *Journal of Molecular Biology*, *413*(1), 247–260. http://doi.org/10.1016/j.jmb.2011.08.014

Brown, P. J. B., de Pedro, M. A., Kysela, D. T., Van der Henst, C., Kim, J., De Bolle, X., et al. (2012). Polar growth in the Alphaproteobacterial order Rhizobiales. *Proceedings of the National Academy of Sciences of the United States of America*, *109*(5), 1697–1701. http://doi.org/10.1073/pnas.1114476109

Cameron, T. A., Zupan, J. R., & Zambryski, P. C. (2015). The essential features and modes of bacterial polar growth. *Trends in Microbiology*, *23*(6), 347–353. http://doi.org/10.1016/j.tim.2015.01.003

Cava, F., de Pedro, M. A., Lam, H., Davis, B. M., & Waldor, M. K. (2011). Distinct pathways for modification of the bacterial cell wall by non-canonical D-amino acids. *The EMBO Journal*, *30*(16), 3442–3453. http://doi.org/10.1038/emboj.2011.246

DeJesus, M. A., Ambadipudi, C., Baker, R., Sassetti, C., & Ioerger, T. R. (2015). TRANSIT - A Software Tool for Himar1 TnSeq Analysis. *PLoS Computational Biology*, *11*(10), e1004401–17. http://doi.org/10.1371/journal.pcbi.1004401

Dhar, N., Bousbaine, D., Wakamoto, Y., McKinney, J. D., & Santi, I. (2013). Single-cell dynamics of the chromosome replication and cell division cycles in mycobacteria.

869   *Nature Communications*, *4*, 1–10. http://doi.org/10.1038/ncomms3470

870 Diacon, A. H., van der Merwe, L., Barnard, M., Groote-Bidlingmaier, von, F., Lange, C.,
871   García-Basteiro, A. L., et al. (2016). β-Lactams against Tuberculosis--New Trick for
872   an Old Dog? *The New England Journal of Medicine*, *375*(4), 393–394.
873   http://doi.org/10.1056/NEJMc1513236

874 Domínguez-Escobar, J., Chastanet, A., Crevenna, A. H., Fromion, V., Wedlich-Söldner,
875   R., & Carballido-López, R. (2011). Processive movement of MreB-associated cell
876   wall biosynthetic complexes in bacteria. *Science*, *333*(6039), 225–228.
877   http://doi.org/10.1126/science.1203466

878 Eskandarian, H. A., Odermatt, P. D., Ven, J. X. Y., Hannebelle, M. T. M., Nievergelt, A.
879   P., Dhar, N., et al. (2017). Division site selection linked to inherited cell surface wave
880   troughs in mycobacteria. *Nature Microbiology*, *2*(9), 17094.
881   http://doi.org/10.1038/nmicrobiol.2017.94

882 Garner, E. C., Bernard, R., Wang, W., Zhuang, X., Rudner, D. Z., & Mitchison, T.
883   (2011). Coupled, Circumferential Motions of the Cell Wall Synthesis Machinery and
884   MreB Filaments in B. subtilis. *Science*, *333*(6039), 222–225.
885   http://doi.org/10.1126/science.1203285

886 Gibson, D. G., Young, L., Chuang, R.-Y., Venter, J. C., Hutchison, C. A., & Smith, H. O.
887   (2009). Enzymatic assembly of DNA molecules up to several hundred kilobases.
888   *Nature Methods*, *6*(5), 343–345. http://doi.org/10.1038/nmeth.1318

889 Global Tuberculosis Report 2017. (2017). Global Tuberculosis Report 2017, 1–262.

890 Gonzalo, X., & Drobniewski, F. (2013). Is there a place for β-lactams in the treatment of
891   multidrug-resistant/extensively drug-resistant tuberculosis? Synergy between
892   meropenem and amoxicillin/clavulanate. *The Journal of Antimicrobial*
893   *Chemotherapy*, *68*(2), 366–369. http://doi.org/10.1093/jac/dks395

894 González-Leiza, S. M., de Pedro, M. A., & Ayala, J. A. (2011). AmpH, a bifunctional DD-
895   endopeptidase and DD-carboxypeptidase of Escherichia coli. *Journal of*
896   *Bacteriology*, *193*(24), 6887–6894. http://doi.org/10.1128/JB.05764-11

897 Gupta, R., Lavollay, M., Mainardi, J.-L., Arthur, M., Bishai, W. R., & Lamichhane, G.
898   (2010). The Mycobacterium tuberculosis protein LdtMt2 is a nonclassical
899   transpeptidase required for virulence and resistance to amoxicillin. *Nature Medicine*,
900   *16*(4), 466–469. http://doi.org/10.1038/nm.2120

901 Hett, E. C., & Rubin, E. J. (2008). Bacterial growth and cell division: a mycobacterial
902   perspective. *Microbiology and Molecular Biology Reviews : MMBR*, *72*(1), 126–56–
903   table of contents. http://doi.org/10.1128/MMBR.00028-07

904 Hugonnet, J.-E., Tremblay, L. W., Boshoff, H. I., Barry, C. E., & Blanchard, J. S. (2009).
905   Meropenem-clavulanate is effective against extensively drug-resistant
906   Mycobacterium tuberculosis. *Science*, *323*(5918), 1215–1218.
907   http://doi.org/10.1126/science.1167498

908 Hussain, S., Wivagg, C. N., Szwedziak, P., Wong, F., Schaefer, K., Izore, T., et al.
909   (2018). MreB filaments align along greatest principal membrane curvature to orient
910   cell wall synthesis. *eLife*, *7*, e32471. http://doi.org/10.7554/eLife.32471

911 Kieser, K. J., & Rubin, E. J. (2014). How sisters grow apart: mycobacterial growth and
912   division. *Nature Publishing Group*, *12*(8), 550–562.
913   http://doi.org/10.1038/nrmicro3299

914 Kieser, K. J., Baranowski, C., Chao, M. C., Long, J. E., Sassetti, C. M., Waldor, M. K., et

915   al. (2015a). Peptidoglycan synthesis in Mycobacterium tuberculosis is organized
916   into networks with varying drug susceptibility. *Proceedings of the National Academy*
917   *of Sciences of the United States of America*, *112*(42), 13087–13092.
918   http://doi.org/10.1073/pnas.1514135112
919 Kieser, K. J., Boutte, C. C., Kester, J. C., Baer, C. E., Barczak, A. K., Meniche, X., et al.
920   (2015b). Phosphorylation of the Peptidoglycan Synthase PonA1 Governs the Rate
921   of Polar Elongation in Mycobacteria. *PLoS Pathogens*, *11*(6), e1005010.
922   http://doi.org/10.1371/journal.ppat.1005010
923 Koschwanez, J. H., Carlson, R. H., & Meldrum, D. R. (2009). Thin PDMS films using
924   long spin times or tert-butyl alcohol as a solvent. *PLoS ONE*, *4*(2), e4572.
925   http://doi.org/10.1371/journal.pone.0004572
926 Kumar, P., Arora, K., Lloyd, J. R., Lee, I. Y., Nair, V., Fischer, E., et al. (2012).
927   Meropenem inhibits D,D-carboxypeptidase activity in Mycobacterium tuberculosis.
928   *Molecular Microbiology*, *86*(2), 367–381. http://doi.org/10.1111/j.1365-
929   2958.2012.08199.x
930 Kuru, E., Hughes, H. V., Brown, P. J., Hall, E., Tekkam, S., Cava, F., et al. (2012). In
931   Situ Probing of Newly Synthesized Peptidoglycan in Live Bacteria with Fluorescent
932   D-Amino Acids. *Angewandte Chemie International Edition*, *51*(50), 12519–12523.
933   http://doi.org/10.1002/anie.201206749
934 Kuru, E., Lambert, C., Rittichier, J., Till, R., Ducret, A., Derouaux, A., et al. (2017).
935   Fluorescent D-amino-acids reveal bi-cellular cell wall modifications important for
936   Bdellovibrio bacteriovorus predation. *Nature Microbiology*, *2*(12), 1648–1657.
937   http://doi.org/10.1038/s41564-017-0029-y
938 Kuru, E., Tekkam, S., Hall, E., Brun, Y. V., & Van Nieuwenhze, M. S. (2014). Synthesis
939   of fluorescent D-amino acids and their use for probing peptidoglycan synthesis and
940   bacterial growth in situ. *Nature Protocols*, *10*(1), 33–52.
941   http://doi.org/10.1038/nprot.2014.197
942 Lavollay, M., Arthur, M., Fourgeaud, M., Dubost, L., Marie, A., Veziris, N., et al. (2008).
943   The Peptidoglycan of Stationary-Phase Mycobacterium tuberculosis Predominantly
944   Contains Cross-Links Generated by L,D-Transpeptidation. *Journal of Bacteriology*,
945   *190*(12), 4360–4366. http://doi.org/10.1128/JB.00239-08
946 Lebar, M. D., May, J. M., Meeske, A. J., Leiman, S. A., Lupoli, T. J., Tsukamoto, H., et
947   al. (2014). Reconstitution of peptidoglycan cross-linking leads to improved
948   fluorescent probes of cell wall synthesis. *Journal of the American Chemical Society*,
949   *136*(31), 10874–10877. http://doi.org/10.1021/ja505668f
950 Long, J. E., DeJesus, M., Ward, D., Baker, R. E., Ioerger, T., & Sassetti, C. M. (2015).
951   Identifying Essential Genes in <Emphasis Type="Italic">Mycobacterium
952   tuberculosis</Emphasis> by Global Phenotypic Profiling. In *Gene Essentiality* (Vol.
953   1279, pp. 79–95). New York, NY: Humana Press, New York, NY.
954   http://doi.org/10.1007/978-1-4939-2398-4_6
955 Mainardi, J.-L., Hugonnet, J.-E., Rusconi, F., Fourgeaud, M., Dubost, L., Moumi, A. N.,
956   et al. (2007). Unexpected inhibition of peptidoglycan LD-transpeptidase from
957   Enterococcus faecium by the beta-lactam imipenem. *Journal of Biological*
958   *Chemistry*, *282*(42), 30414–30422. http://doi.org/10.1074/jbc.M704286200
959 Murphy, K. C., Papavinasasundaram, K., & Sassetti, C. M. (2015). Mycobacterial
960   recombineering. *Methods in Molecular Biology (Clifton, N.J.)*, *1285*, 177–199.

961 http://doi.org/10.1007/978-1-4939-2450-9_10

962 Paintdakhi, A., Parry, B., Campos, M., Irnov, I., Elf, J., Surovtsev, I., & Jacobs-Wagner,
963 C. (2016). Oufti: an integrated software package for high-accuracy, high-throughput
964 quantitative microscopy analysis. *Molecular Microbiology*, *99*(4), 767–777.
965 http://doi.org/10.1111/mmi.13264

966 Papp-Wallace, K. M., Endimiani, A., Taracila, M. A., & Bonomo, R. A. (2011).
967 Carbapenems: past, present, and future. *Antimicrobial Agents and Chemotherapy*,
968 *55*(11), 4943–4960. http://doi.org/10.1128/AAC.00296-11

969 Pisabarro, A. G., de Pedro, M. A., & Vázquez, D. (1985). Structural modifications in the
970 peptidoglycan of Escherichia coli associated with changes in the state of growth of
971 the culture. *Journal of Bacteriology*, *161*(1), 238–242.

972 Qiao, Y., Lebar, M. D., Schirner, K., Schaefer, K., Tsukamoto, H., Kahne, D., & Walker,
973 S. (2014). Detection of lipid-linked peptidoglycan precursors by exploiting an
974 unexpected transpeptidase reaction. *Journal of the American Chemical Society*,
975 *136*(42), 14678–14681. http://doi.org/10.1021/ja508147s

976 Qiao, Y., Srisuknimit, V., Rubino, F., Schaefer, K., Ruiz, N., Walker, S., & Kahne, D.
977 (2017). Lipid II overproduction allows direct assay of transpeptidase inhibition by β-
978 lactams. *Nature Chemical Biology*, *13*(7), 793–798.
979 http://doi.org/10.1038/nchembio.2388

980 Rebets, Y., Lupoli, T., Qiao, Y., Schirner, K., Villet, R., Hooper, D., et al. (2014).
981 Moenomycin resistance mutations in Staphylococcus aureus reduce peptidoglycan
982 chain length and cause aberrant cell division. *ACS Chemical Biology*, *9*(2), 459–
983 467. http://doi.org/10.1021/cb4006744

984 Rego, E. H., Audette, R. E., & Rubin, E. J. (2017). Deletion of a mycobacterial divisome
985 factor collapses single-cell phenotypic heterogeneity. *Nature*, *546*(7656), 153–157.
986 http://doi.org/10.1038/nature22361

987 Sanders, A. N., Wright, L. F., & Pavelka, M. S. (2014). Genetic characterization of
988 mycobacterial L,D-transpeptidases. *Microbiology (Reading, England)*, *160*(Pt 8),
989 1795–1806. http://doi.org/10.1099/mic.0.078980-0

990 Schindelin, J., Arganda-Carreras, I., Frise, E., Kaynig, V., Longair, M., Pietzsch, T., et
991 al. (2012). Fiji: an open-source platform for biological-image analysis. *Nature
992 Methods*, *9*(7), 676–682. http://doi.org/10.1038/nmeth.2019

993 Synergism Testing: Broth Microdilution Checkerboard and Broth Macrodilution Methods.
994 (2016). Synergism Testing: Broth Microdilution Checkerboard and Broth
995 Macrodilution Methods. In *Clinical Microbiology Procedures Handbook, Fourth
996 Edition* (pp. 5.16.1–5.16.23). American Society of Microbiology.
997 http://doi.org/10.1128/9781555818814.ch5.16

998 Thangawng, A. L., Ruoff, R. S., Swartz, M. A., & Glucksberg, M. R. (2007). An ultra-thin
999 PDMS membrane as a bio/micro-nano interface: fabrication and characterization.
1000 *Biomedical Microdevices*, *9*(4), 587–595. http://doi.org/10.1007/s10544-007-9070-6

1001 Ursell, T. S., Nguyen, J., Monds, R. D., Colavin, A., Billings, G., Ouzounov, N., et al.
1002 (2014). Rod-like bacterial shape is maintained by feedback between cell curvature
1003 and cytoskeletal localization. *Proceedings of the National Academy of Sciences of
1004 the United States of America*, *111*(11), E1025–34.
1005 http://doi.org/10.1073/pnas.1317174111

1006 Vollmer, W., Blanot, D., & de Pedro, M. A. (2008a). Peptidoglycan structure and

58

1007   architecture. *FEMS Microbiology Reviews*, *32*(2), 149–167.
1008   http://doi.org/10.1111/j.1574-6976.2007.00094.x
1009 Vollmer, W., Joris, B., Charlier, P., & Foster, S. (2008b). Bacterial peptidoglycan
1010   (murein) hydrolases. *FEMS Microbiology Reviews*, *32*(2), 259–286.
1011   http://doi.org/10.1111/j.1574-6976.2007.00099.x
1012 Welsh, M. A., Taguchi, A., Schaefer, K., Van Tyne, D., Lebreton, F., Gilmore, M. S., et
1013   al. (2017). Identification of a Functionally Unique Family of Penicillin-Binding
1014   Proteins. *Journal of the American Chemical Society*, *139*(49), 17727–17730.
1015   http://doi.org/10.1021/jacs.7b10170
1016 Zimmermann, L., Stephens, A., Nam, S.-Z., Rau, D., Kübler, J., Lozajic, M., et al.
1017   (2017). A Completely Reimplemented MPI Bioinformatics Toolkit with a New
1018   HHpred Server at its Core. *Journal of Molecular Biology*.
1019   http://doi.org/10.1016/j.jmb.2017.12.007
1020